INTERFACIAL SYNTHESIS OF MOF

INTERFACIAL SYNTHESIS OF METAL-ORGANIC FRAMEWORKS

By HONGYU LU, B.A.

A Thesis Submitted to the School of Graduate Studies in Partial Fulfilment of the Requirements for the Degree Master of Applied Science

McMaster University MASTER OF APPLIED SCIENCE (2012)

Hamilton, Ontario (Chemical Engineering)

TITLE: Interfacial Synthesis of Metal-organic Frameworks

AUTHOR: Hongyu Lu, B.A. (Tsinghua University, Beijing, PRC)

SUPERVISOR: Professor Shiping Zhu

NUMBER OF PAGES: xiii, 70

ABSTRACT

Metal-organic frameworks (MOFs) are considered as a type of very useful materials for the gas separation/purification industries. However, control over the growing position and growing shape of the crystals remains a challenge and must be overcome in order to realize the commercial potentials of MOFs.

In this thesis, a method based on interfacial coordination is developed to address this issue. Zinc-benzenedicarboxyl (Zn-BDC) is chosen as a model system for the proof of concept. In a typical liquid-liquid interface protocol, the MOF precursors, zinc nitrate $[Zn(NO_3)_2]$ and terephthalic acid (TPA or H_2BDC), and the catalyst, triethylamine (TEA), were dissolved into two immiscible solvents, dimethylformamide (DMF) and hexane, respectively. The reaction site, i.e. the MOF growing position could thereby be confined at the interface of the two solvents. It was found that a free-standing membrane could be formed with the combinations of high Zn-H_2BDC and low TEA concentrations. The combinations of low Zn-H_2BDC and high TEA concentrations yielded MOF particles precipitated out from DMF.

Similar results were obtained by changing the liquid-liquid interface to liquid-gas interface, with the TEA-hexane solution replaced by saturated TEA vapor.

The dependence of product shape on precursor and catalyst concentrations can be explained by the competition between MOF formation and TEA diffusion into the precursor phase.

The morphology, constitution and surface area of the MOF products were characterized by SEM, XRD and nitrogen adsorption testing, respectively. The particles were found to be exclusively MOF-5. The membranes were characterized as asymmetric. The top layer was particulate while the bottom layer had a sheet-like morphology. This was further revealed by XRD data as MOF-5 and MOF-2 (ZnBDC·DMF), respectively. This asymmetry was caused by a change of TEA diffusion rate during the synthesis process, which might result in a change in pH value for the membrane growth. Decent surface areas of the particles and membranes were measured.

Apart from the free-standing membranes, MOF membranes on Anodisc support were also synthesized employing the same interfacial techniques. The MOF formation site, i.e. the interface, was confined to the upper end Anodisc pores and sealing the pores after the reaction. The difference in wetting force between DMF and hexane with Anodisc membrane material resulted in the difference of MOF layer morphology from liquid-liquid protocol and liquid-gas protocol. The later gave a continuous MOF membrane due to the absence of air bubble interference.

AKNOWLEDGEMENTS

To Dr. Jerry (Y.-S.) Lin and Dr. Jose Ortiz Landeros from Arizona State University, I thank you for helping me with gas adsorption test.

To the staff in Chemical Engineering, Nancy Cole (now in Materials Engineering), Lynn Falkiner, Kathy Goodman and Melissa Vasil, thank you for your kind help.

Last but not least, to my parents, Mrs. Zhang Yongfeng and Mr. Lu Mingquan, and others who love me and care about me from my family, thank you all for your understanding and support.

TABLE OF CONTENTS

List of Figures

Chapter 3

Chapter 5

List of Schemes

List of Tables

Chapter 1 Introduction

1.1 Metal-organic frameworks

Metal-organic frameworks (MOFs) are a new class of materials, which have been intensely studied in the recent years. A typical MOF comprises metal ions connected by organic bridges forming well-defined repeating frameworks.   A list of most often studied MOFs is given in Table 1.1.

The discovery and development of MOFs stand out as a groundbreaking progress because these materials possess the crystalline regularities of inorganic materials while simultaneously maintaining the flexibility of functional modifications on their organic bridges.   The topologies can be varied by manipulating the coordination styles between metal ions and organic dents or by changing the number of dents on organic bridges.   The pore size can be tuned by choosing organic monomers with different size of backbones.   Even the chemistry of the material can be manipulated delicately by grafting reactive groups to the frameworks.   Due to these unique merits, MOFs possess high potentials for applications in such areas as separation, filtration, catalysis and gas storages.

Table 1.1 List of commonly seen MOFs

Names	Moieties	Metal-organic bridge coordination style	Unit cell shape
MOF-5	Zn^2+, benzene dicarboxylate:	Tetragon: four ZnO_4 tetragons form a larger tetragon by sharing one mutual free oxygen, other oxygens come from carboxylate groups	Cubic
HKUST-1	Cu^2+, benzene tricarboxylate:	Binuclear: two Cu^2+ coordinate with eight oxygens from four carboxylate groups	Cubic
ZIFs (ZIF-7, ZIF-8, ZIF-9, ZIF-11)	Zn^2+, Co^2+ and imidazolate:	ZnN_4 tetragon or CoN_4 tetragon	Sodalite

1.2 MOF for gas separations

When conventional dense membranes are used for gas separations, the solubility difference of gas molecules into the membrane material serves as the drive for separation. However, this set a critical trade-off between selectivity (separation quality) and permeability (energy consumption or cost): large thickness of membrane

is required for good separation, but gas permeation resistance would increase with
membrane thickness. (Figure 1.1 a)
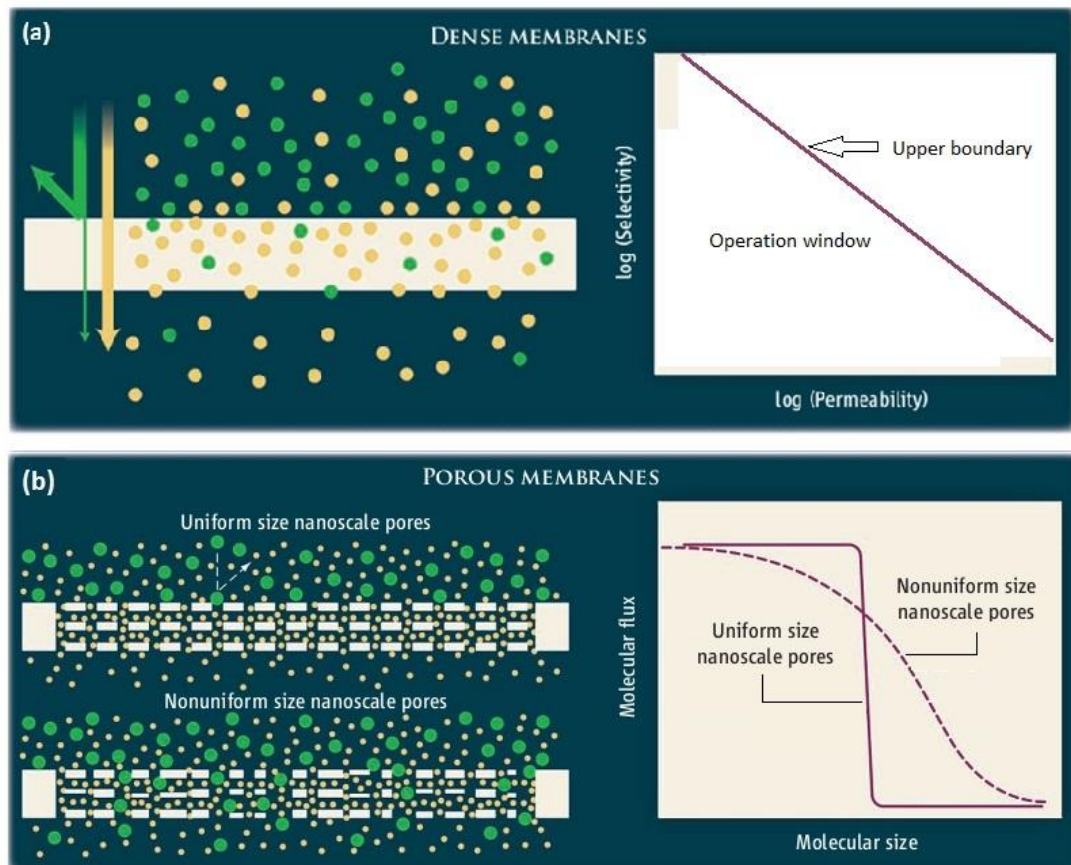
Figure 1.1 Separation patterns for (a): dense membranes and (b): porous membranes
(Gin and Noble, 2011)

Compared to dense membranes, membranes made from porous materials can
break through such boundary by selecting molecules with sizes smaller than pore
diameter exclusively to pass through the membrane, which is also referred to as size
exclusive effect.   When the pores are uniform, such selectivity can be very sharp,

indicating 100% separation for gas mixtures with molecule sizes ranging from lower than pore diameter to larger than pore diameter, which is the most ideal situation. Porous membranes with non-uniform pores can still separate gas mixtures, however, non-uniform pores provide by-pass for larger molecules, which impose a limit to the quality of separation.   In this case, the difference of diffusion rate between molecules passing through the membrane serves as primary drive for separation. This mechanism is also referred to as Knudsen effect (Figure 1.1 b).

Table 1.2 Summary of membrane separations

Membrane type	Drive	Drive force type	Separation quality
Dense membrane	Kinetic, solubility difference	Chemical	Not sharp
Non-uniform porous membrane	Kinetic, diffusion rate difference	Physical	Not sharp
Uniform porous membrane	Thermodynamic, size-exclusive	Physical	Sharp

A comparison between different separative membranes is given in Table 1.2. As we can see, porous membrane with uniform pore sizes gives the best results. Before the development of MOFs, Zeolite, a group of aluminosilicate materials, has been considered as good materials to fabricate such membranes, and there have been news for industrialization already.   However, available pore sizes of Zeolite are very limited, which means they can only separate certain types of gas mixtures.   For

MOFs, there is no such limit.   The selection of precursors and control of coordination types provide almost unlimited choices for pore topologies, sizes and chemistries, which give them high potential as gas-separation materials.

1.3 MOF based membranes

1.3.1 Synthesis of MOF and challenges involved in MOF membrane fabrication

Solvothermal method is by far the most commonly used approach in the synthesis of MOF materials.   In a typical solvothermal protocol, solution containing the precursors of MOF formation, i.e. metal ions and organic bridges, is heated under a certain temperature to allow crystal growth to occur.   It is found that for some protocols, heat can be replaced by other stimulus, such as ultrasound, microwave and electrical field (electrochemical deposition).   Methods other than solvothermal include the room temperature catalysis (MOF-5 nano-particles), non-solvent precipitation (HKUST-1), gel formation-crystallization (iron based MOFs, such as MIL-79) etc.

All the MOF synthesis methods developed to date generate MOFs in particulate forms.   This raises a major challenge when we are trying to use these materials in gas separation applications where membranes are always required.   It is difficult to grow these materials into shapes other than their natural particulate form,

termed as 'grow in shape'. It is also difficult to direct the growth into a certain position where it can form part of a membrane, termed as 'growing to position'. By far, most of the efforts made in overtaking these problems have concentrated in two directions, growth of MOFs on a surface in-situ or by seeding-secondary growth approach, and fabrication of mixed-matrix membranes by blending already synthesized MOF particles with other structural materials, generally polymers.

1.3.2 In-situ and seeding-secondary growth of MOF membranes

In this general direction, a target surface is demanded as a template for MOF growth. The surface is modified or processed to make it compatible with MOF growth, that is, by introducing active groups which can interact with the metal ions or organic groups on MOF surface. Interactions with metal ions are preferred as negatively charged organic groups are widely used as grafting functional groups (Figure 1.2). Then the template is put into a mother solution to let in-situ growth of MOF occur on the surface, i.e. in-situ growth, or MOF seeds are transferred onto the surface followed by a secondary solvothermal growth step, i.e. seeding-secondary growth.
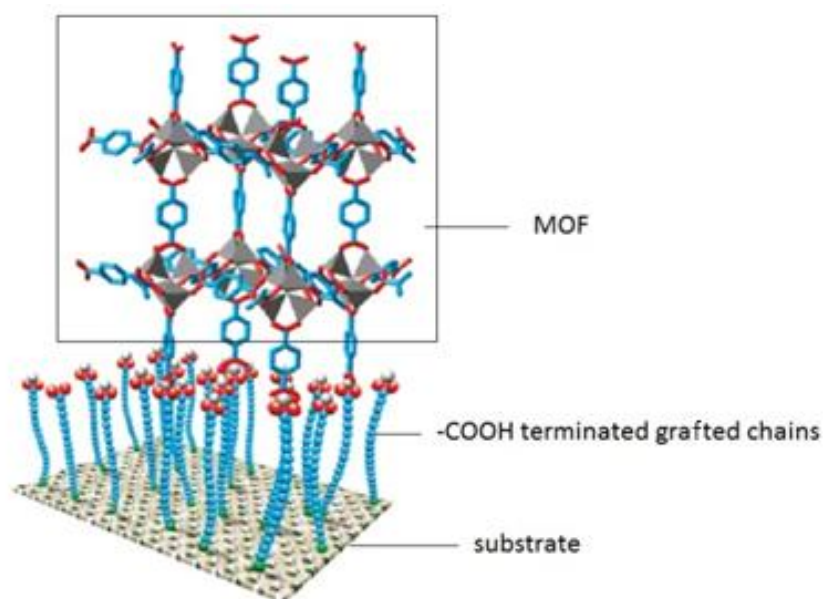
Figure 1.2 The concept of surface modification to increase compatibility
with MOF (Hermes et al., 2005)

In 2005, Hermes et al. grew MOF-5 thin films on gold substrate by introducing a -COOH or -CF_3 terminated self-assembled monolayer (SAM) on top of the gold plate to induce MOF growth, which was likely to be the first work reported on templating MOF growth on flat surface. In their work, when the SAM was prepared in a matrix manner, a corresponding MOF matrix was produced (Figure 1.3). Although not to a very precise location, this also indicated a method of 'growing to position'.
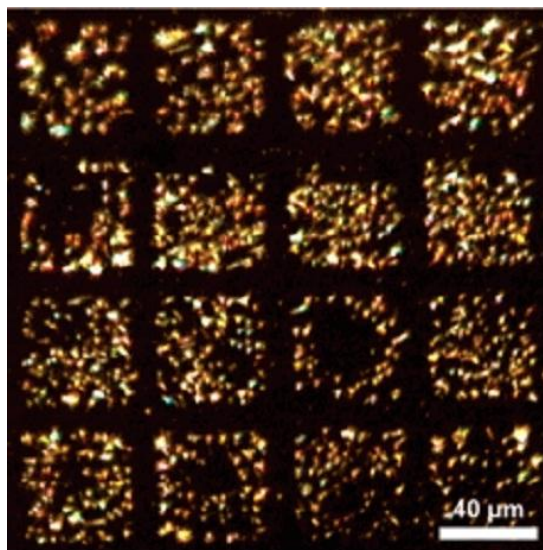
Figure 1.3 MOF-5 matrix on gold substrate, black areas were not covered with SAM
(Hermes et al., 2005)

Yoo and Jeong (2008) reported rapid fabrication of MOF membrane using microwave-induced thermal deposition.   MOF-5 seeded Anodisc membrane was immersed into a precursor solution and was then ultrasonicated for 5-30s.   The time period in seconds was much less than the hours needed using the conventional methods.   They also found that by grafting the substrate surface with graphite, a better membrane quality was obtained.   As graphite is not compatible with MOF-5 from chemistry perspective, the only way to explain this is that rapid temperature increase of graphite under microwave can induce a solvothermal precipitation of MOF-5.

Arnold et al. (2007) succeeded with in-situ growth of manganese formate $[Mn(HCO_2)_2]$ on porous alumina and graphite from a solvothermal solution. High

crystal density on alumina surface was achieved by pre-treating the surface with NaOH to enrich –OH groups.   They also reported that the orientation of [Mn(HCO$_2$)$_2$]'s 1-D channel tends to parallel to that of the substrate surface (Figure 1.4).   Despite MOF crystals were not continuous on the substrate, this was the first report that the orientation of MOFs can be controlled.
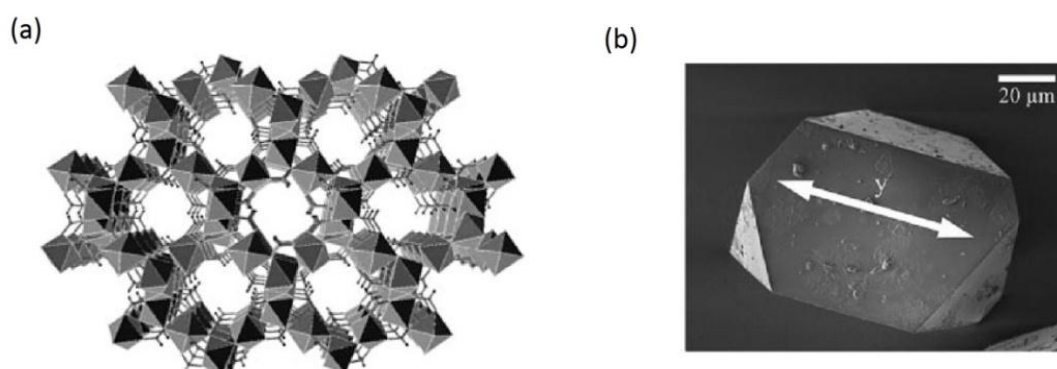
Figure 1.4   Schematic drawing of the 1-D channel inside [Mn(HCO$_2$)$_2$] crystal (a) and the oriented alignment of such channels along substrate surface ('y' axis in Sub-figure b) (Arnold et al., 2007)

Gascon et al. managed to update the frontier of MOF quality in late 2007 by reporting a densely coated of Cu$_3$(BTC)$_2$ (or HKUST-1) on alumina support, where alumina disc surface was seeded prior to secondary MOF growth.   Although still not continuous, the cracks between MOF grains become much less.   Soon after this, Guo et al. showed that HKUST-1 could also be densely deposited on pre-oxidized copper net surface by in-situ solvothermal growth.

In 2009, Liu et al. synthesized continuous and uniform MOF-5 membrane by

9

dipping a pre-treated alumina disk into a mother solution followed by solvothermal synthesis, which was probably the first continuous MOF membrane obtained (Figure 1.6 b). This marked a milestone which presented the first example of MOF membranes that could actually demonstrate gas separation. From hydrogen permeation tests, they measured permeability values close to theoretical ones. This experimentally proved that the properties of MOFs can be well predicted based on their cell structures.

Soon after that, Li and Caro et al. (2010) also obtained continuous membranes of ZIF-7 on alumina support and ZIF-8 on titanium support through a microwave-assisted solvothermal synthesis route. Zhao et al. successfully grew a MOF-5 membrane from an α-alumina support by pre-seeding the surface with a MOF-5 suspension.

Recently, attention starts to be paid to more delicately manipulate of membrane morphology, which is the growing direction of MOFs on surface. In 2010, Li et al. obtained oriented ZIF-7 membranes by employing van der Drift type growth on a random-orientation seed layer. By manipulating the ratio between precursors and amine (catalyst), they managed to confine MOF growth to certain crystal faces, resulting in rod-shaped grains, which would align vertically to the substrate surface by van der Drift effect (Figure 1.5). ZIF-8 oriented MOF was also reported later by the same group employing a similar mechanism (Bux et al., 2011).
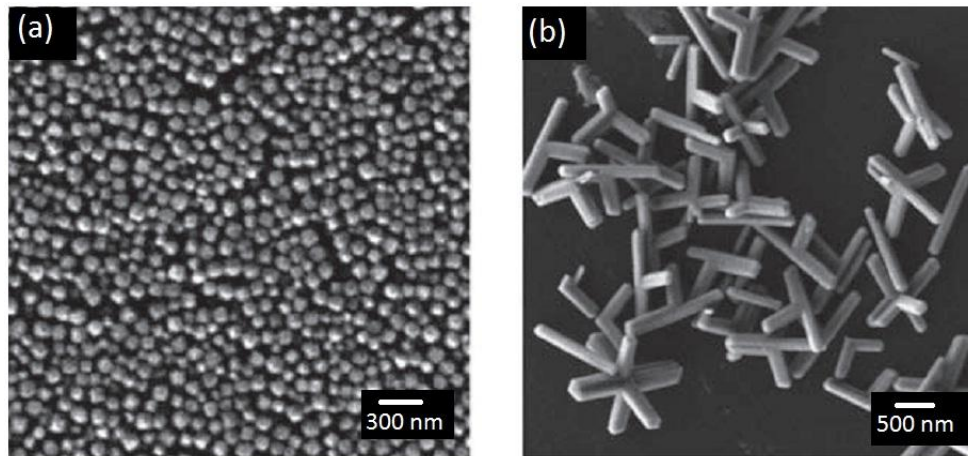
Figure 1.5 (a) Top view of ZIF-7 grains on substrate; (b) Individual grains (Li et al., 2010)

As we can see, synthesis of the above oriented MOF layer requires good understanding about the thermodynamics of MOF growth patterns. In Yoo et al.'s method (2009), such concern was overcome by simply rubbing MOF-5 seeds on the substrate surface, which resulted in oriented MOF grains after solvothermal growth (Figure 1.6 c). This approach would not work with ZIFs as their crystal seeds did not orient under rubbing due to their rod-like shape.

From the above literature, we can see the evolution pattern on the quality of in-situ grown MOF membranes, that is, from surface grafting to continuous MOF layer, and then to oriented MOF layer, as shown in Figure 1.6.
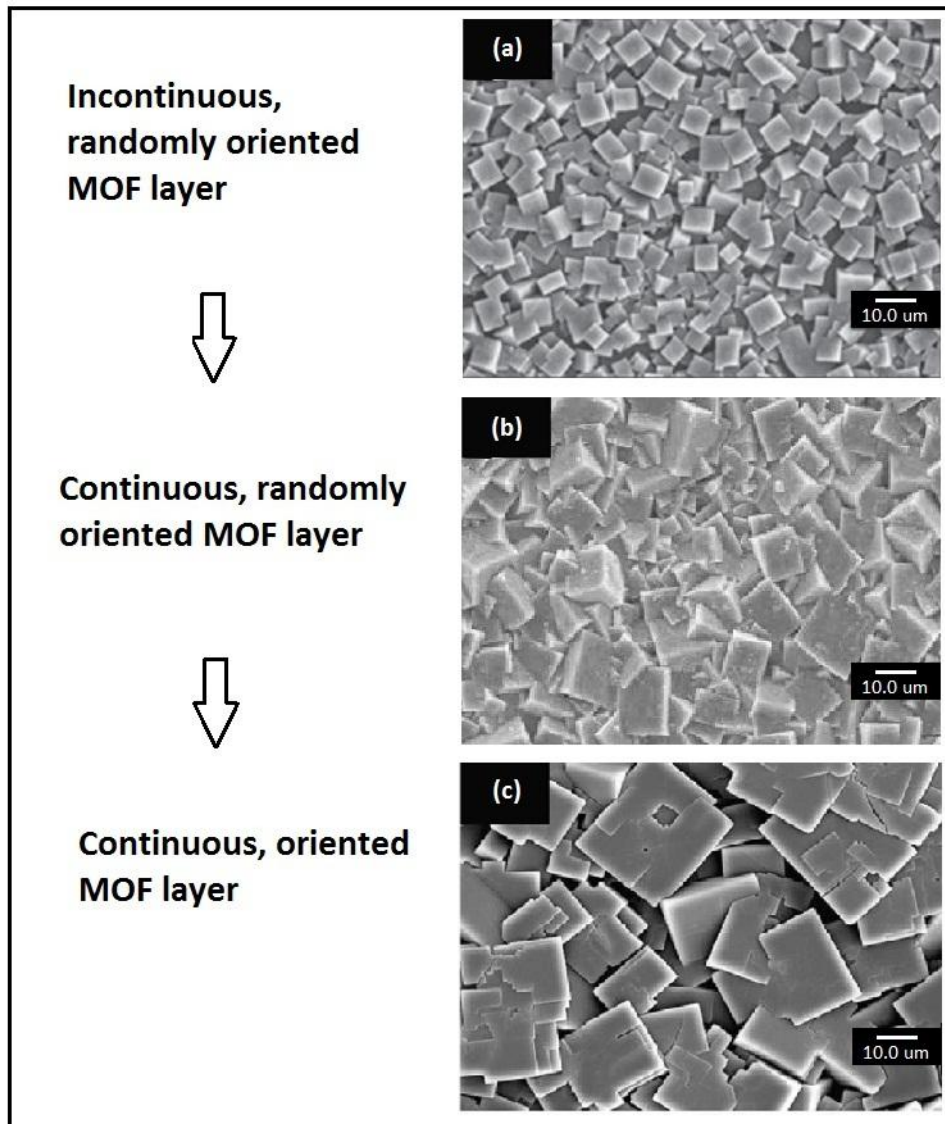
Figure 1.6 The evolvement of supported MOF membranes.   The SEM images show MOF-5 on top of supports. (Yoo and Jeong, 2008, 2009; Liu et al. 2009)

The problem involved in this approach is that the majority of MOF growth occurs inside mother solution, rather than on substrate surface.   The later can only account for a very small proportion the total MOF produced (<5%).   This is not only a waste of material, the disturbance introduced by solution nucleation and MOF

growth also results in low density and poor attachment of MOF on the membrane. A similar problem was also observed in synthesizing zeolites, which is a group of inorganic materials sharing quite similar structures such as MOFs. Note: a sub-group of MOFs, i.e. ZIFs were actually developed by employing the topologies of zeolites. Although a protocol without solution nucleation for zeolite synthesis was eventually found by Cao et al. in 2011 after a so claimed more than one thousand experiments, there is no sign yet that such a protocol can be found easily in the MOF area.

1.3.3 Mixed-matrix membranes

Mixed-matrix membranes (MMMs) are a category of composite membranes consisting of fillers dispersed in matrix materials. For gas separation, using zeolites and polymers to fabricate MMMs has been widely studied with some good results achieved. These works have provided a solid foundation for explorations of MOF-based MMMs.

Up to date, there have been several tries on this topic. Hu et al. (2010) reported the synthesis of HKUST-1/polyimide MMM hollow fibers using dry/wet-spinning method. This method was commonly used to produce polyimide membranes with asymmetric pore structures. An interesting observation about their products was the opposite change in selectivity regarding to hydrogen and

carbon-dioxide with the increase of MOF load (Figure 1.7).   Since the size of HKUST-1 pore size lies in between the sizes of hydrogen and carbon-dioxide molecules, this can be explained by the switch of permeation mechanism from size-exclusion in the case of hydrogen to Knudsen diffusion in the case of carbon dioxide.
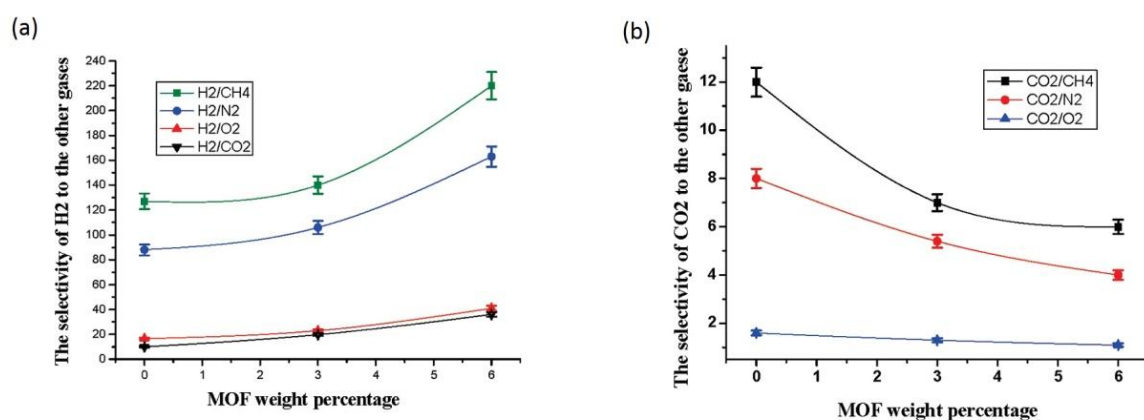
Figure 1.7 Selectivties of (a): hydrogen and (b): carbon dioxide against methane, nitrogen and oxygen in HKUST-1-PI composite membrane (Hu et al., 2010)

Adams et al. (2010) synthesized HKUST-1/polyvinyl acetate composite membranes via polymer solution processing.   Good compatibility between HKUST-1 and PVAc was observed with HKUST-1 loading up to 15 wt%.

Basu et al. (2010, 2011) used a similar polymer solution method and prepared MMMs with Matrimid® as matrix and HKUST-1, ZIF-8 or MIL-53 as fillers.   They also explored a phase-inverse method to obtain asymmetric Matrimid®/HKUST-1 MMMs.   Declining mechanical performances of MMMs with the increase of MOF

load were evident in their results as shown in Table 1.3.

Synthesis of Matrimid®-based MMMs where MOF-5 was used as the filler was also reported by Perez (2009). Liu et al. (2010) reported that ZIF-8-polymethylphenylsiloxane MMMs showed exceptional selectivity toward bio-alcohols.

Table 1.3   Mechanical properties of MMMs at different MOF loadings (Basu et al., 2010, 2011)

MOF/PI	MOF loading (w/w)	Young modulus (GPa)	Tensile strength (MPa)	Elongation at break (%)
[Cu$_3$(BTC)$_2$]	0%	2.5 ± 0.1	105 ± 2	119 ± 2
	10%	2.86 ± 0.2	96 ± 4	100 ± 3
	20%	3.33 ± 0.4	75 ± 3	86 ± 4
	30%	3.62 ± 0.35	61 ± 2	66 ± 5
MIL–53(Al)	0%	2.5 ± 0.1	105 ± 2	119 ± 2
	10%	2.72 ± 0.3	82 ± 5	103 ± 2
	20%	3.25 ± 0.3	71 ± 3	92 ± 4
	30%	3.54 ± 0.4	66 ± 2	66 ± 5
ZIF-8	0%	2.5 ± 0.1	105 ± 2	119 ± 2
	10%	2.91 ± 0.2	90 ± 4	104 ± 3
	20%	3.42 ± 0.5	73 ± 5	86 ± 4
	30%	3.63 ± 0.6	61 ± 3	65 ± 3

The key issue in this general approach, which is not different from all other MMM fabrications, is to improve the compatibility between MOFs and matrix materials. Polymers such as polysulphone, polyimide and Matrimid® were widely used as matrix material mainly because of their interactivity with MOF moieties (Figure 1.8).

Due to the crystalline rigidity of MOF fillings, declining mechanical

performances of membranes were commonly observed with the increase of MOF proportion inside the membrane.   Typical maximum MOF loadings reported were in the range of 15 to 40 wt%.   Above the load limits, membranes can become so fragile that they break even in the process of drying.   Compared to the supported membranes reviewed above, it is also unlikely that a clear and isolated MOF layer can be found inside MOF MMMs.   The matrix materials would either provide by-pass for gas penetration or cover the functionality of MOF materials.   Figure 1.9 gives an example of HKUST-1 and Matrimid$^{®}$ (Vankelecom et al., 2010).   By-passes provided by the pores inside the matrix material and the gaps between MOF and matrix material were evident.   Thus, this approach was commonly employed to improve the permeability and/or selectivity of existing separative polymer membranes rather than making a membrane where MOF can function independently.   Due to this limit, the separation can only be based on Knudson effect, that is, to separate gases based on their rate differences in passing through channels across a membrane.   Higher selectivity can generally be obtained in the supported MOF membranes where the pore sizes of MOFs can be employed to select a certain gas passing through the membrane, that is, to have size-exclusive effect involved.   Thus, despite that MOF MMMs use more mature and simpler techniques, their potential is more limited than the membranes consisting of a continuous MOF layer.

16
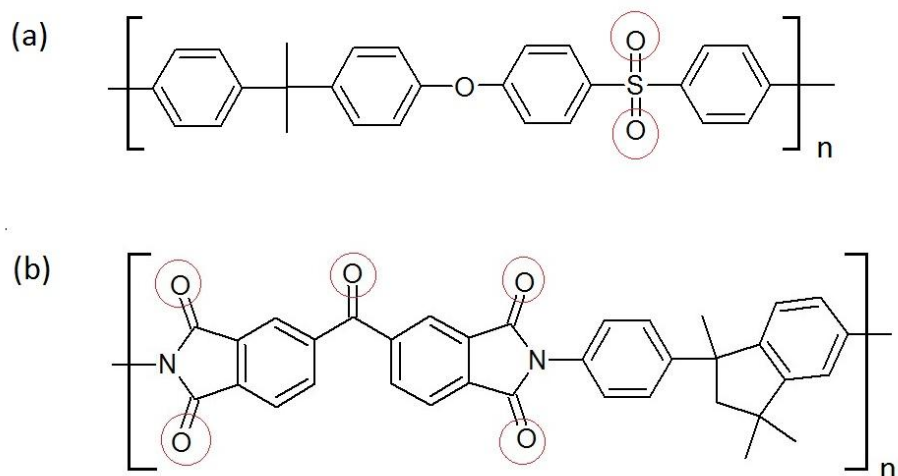
Figure 1.8 Polysulphone (a) and Matrimid® (b) and their functional groups that can interact with MOF metal ions (marked in red)
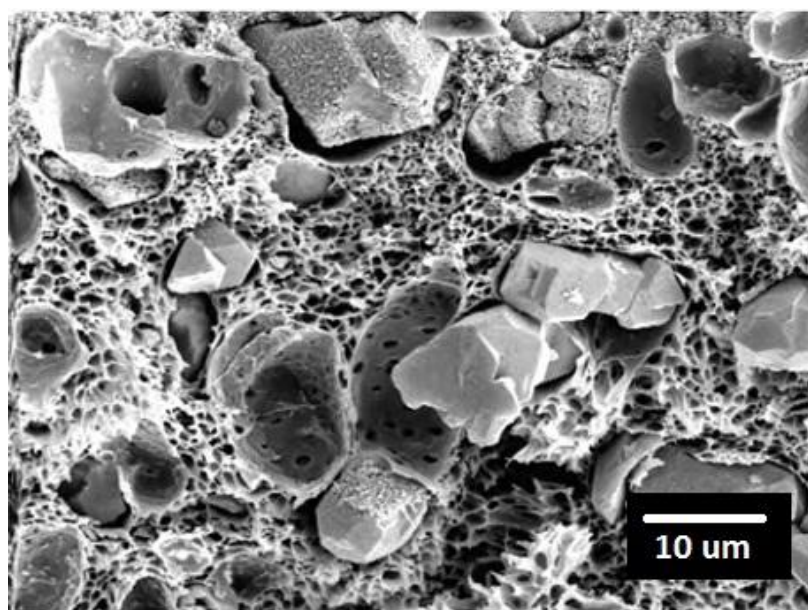
Figure 1.9 SEM of HKUST-1 - Matrimid® MMM (Vankelecom et al., 2010)

17

1.3.4 Other methods

Although not in the main streams, methods other than those mentioned above for fabricating MOF membranes have been explored and significant progress has been made.

Yao et al. (2011) reported the synthesis of ZIF-8-nylon composite membranes using a contra-diffusion approach (Figure 1.10).   The precursors are separated into two independent solutions on different sides of a nylon membrane, crystal growth was allowed to happen while the two precursors met inside the membrane.   This work can be viewed as an extension of Lin et al.'s reported technique of synthesizing silica membranes (Lin et al., 2009).
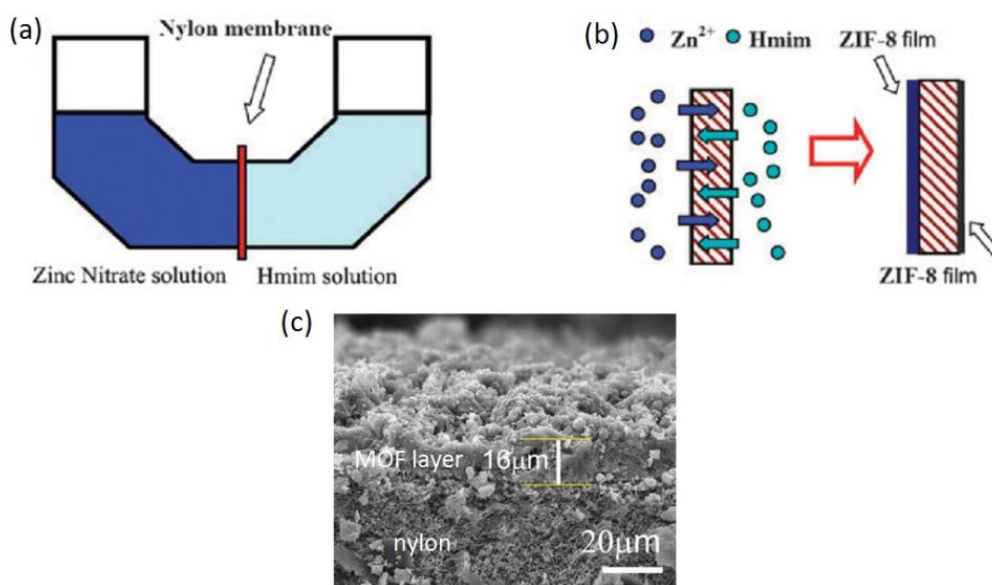
Figure 1.10 Contra-diffusion synthesis of ZIF-nylon composite membrane.   (a): the diffusion cell, (b): the scheme of MOF formation, and (c): SEM of membrane cross-section (Yao et al. 2011)

Shekah et al. (2007, 2010) reported deposition of a HKUST-1 layer on supporting membrane by dipping the substrate alternatively into the organic and metal-ion precursor solutions.   A layer-by-layer growth pattern of MOF was observed, demonstrating an effective way to control MOF layer thickness.   Since the obtained MOF layer was very thin, it was later found by Nan et al. (2011) that it is possibly more suitable for seeding a surface before solvothermal growth.

Electrochemical reduction was also reported by Li et al. (2011) as an approach to obtain MOF layers.   In their work, the role of triethylamine (TEA) in the conventional synthesis of MOF-5 was replaced by OH^- produced from reduction of NO_3^- anions, which provided a deprotonator for the acid precursor, terephthalic acid. MOF formation on the surface of the anode then occurred (Figure 1.11).
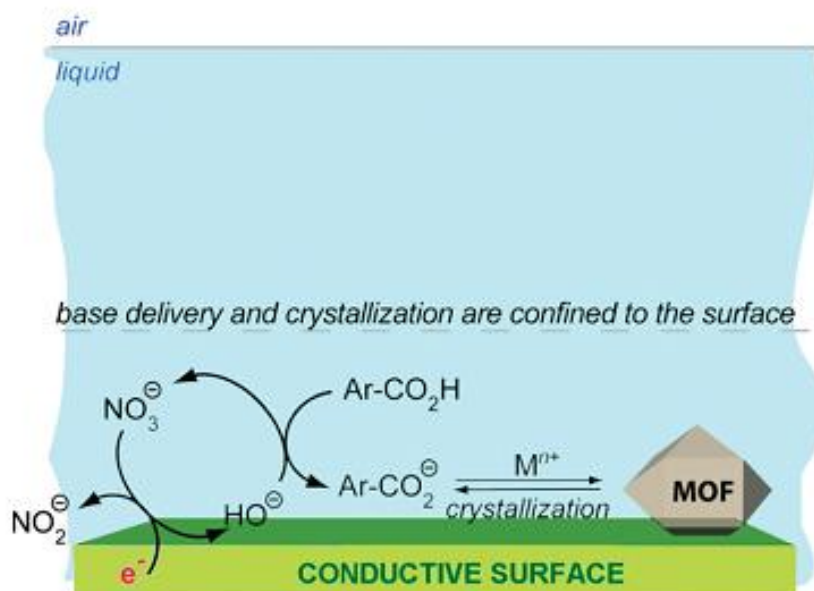
Figure 1.11   Reductive production of MOF layer on an anode surface (Li et al., 2011)

19

Another work worth mentioning here, despite that it was not really making MOF membranes, is the fabrication of single crystal arrays by Carbonell et al. (2011). In their work, a precursor solution of HKUST-1 was injected precisely on a substrate surface using a pen-type lithography technique. Crystallization occurred when solvent evaporated, resulting in precisely aligned MOF arrays (Figure 1.12) This simple and effective operation has provided a new perspective on how to control the growth position of MOFs.
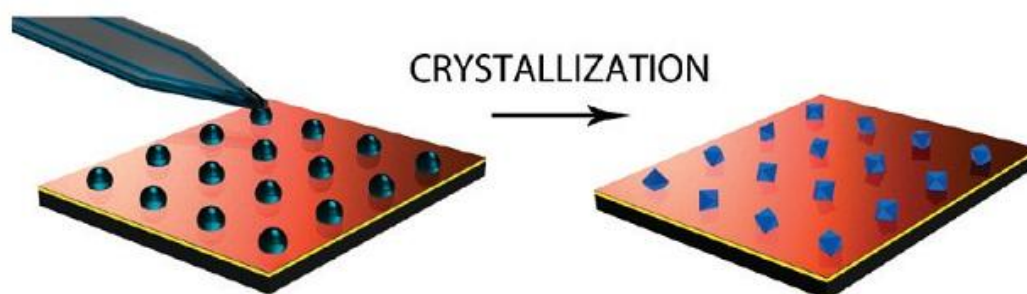
Figure 1.12 Controlling growth position of HKUST-1 on gold substrate (Carbonell et al., 2011)

1.4 Interfacial polymerization and coordination

Interfacial polymerization is a unique technique developed for polymer fabrication. It is suitable for synthesizing polymers with a -AA-BB-AA- chain structure through condensation. In a typical protocol, monomers AAs and BBs are dissolved into two immiscible solvents, respectively. The polymerization then occurs at the solvent interface (Figure 1.13).
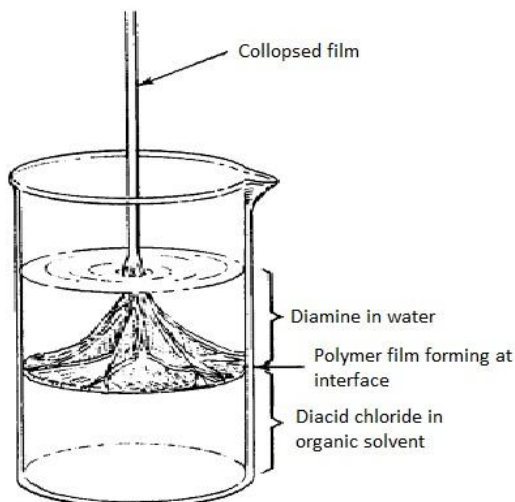
Figure 1.13 Interfacial polymerization of nylon (polyamide) (Odian, 2004)

The advantage, which is also a pre-requisite for an interfacial polymerization, is that the monomers react with the growing polymer chains at the interface before they diffuse into the other side, thus high molecular weight products can be achieved. A high reaction rate at the interface is required.   This requirement, plus the solubility and chain structural consideration, has limited the use of this technique to fabrication of polyesters and polyamines (nylons) only (Figure 1.14).
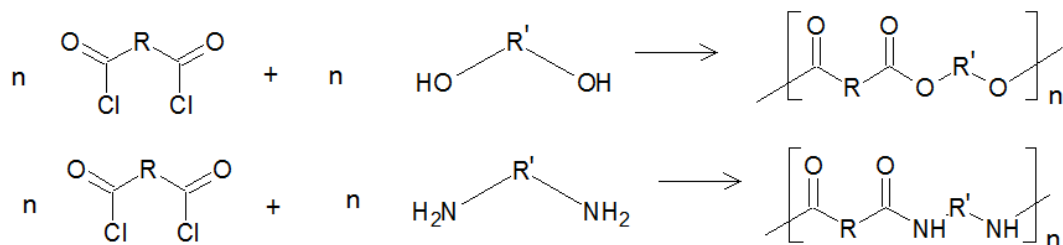
Figure 1.14 Interfacial polymerization reactions

1.5 Zinc-benzenedicarboxylate based MOFs

Zinc-benzenedicarboxylate (Zn-BDC) based MOFs represent a very important sub-group of MOFs.   The coordination between zinc ions and carboxylate groups of BDC laid the foundation of these materials (Figure 1.15).   The four oxygen atoms from each BDC group have an equal reactivity after deprotonation.
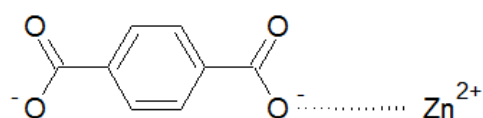
Figure 1.15 Coordination between BDC and zinc ions

The most often seen and well studied Zn-BDC MOF is MOF-5.   MOF-5 has the chemical formula of $Zn_4O(BDC)_3$ and the unit cell as shown in Figure 1.16. ZnO_4 tetragons form a larger tetragon by sharing one oxygen, making up the vertexes of a cubic-shaped unit cell.   The pore size of this MOF (marked in yellow) under an ideal situation, that is, no filling of solvent molecules, is 15.20 angstroms.
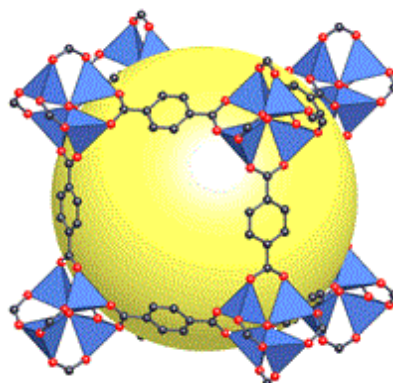
Figure 1.16 Unit cell of MOF-5. Black: carbon; red: oxygen; blue: ZnO_4 tetragon;yellow: pore space (Yaghi, 2007)

In the first synthesis protocol of MOF-5 reported by Yaghi (1998), triethylamine (TEA) was added slowly into diethylformamide (DEF) solution containing zinc nitrate hexahydrate $Zn(NO_3)_2 \cdot 6H_2O$ and terephthalic acid (H_2BDC) at room temperature.   By adding TEA in a faster manner accompanied by stirring, Huang et al. reported the synthesis of MOF-5 nanoparticles.   In this protocol, TEA works as a deprotonator to activate the coordination between carboxyl groups and zinc ions.   Based on this process, solvothermal protocols, where only precursors [still $Zn(NO_3)_2 \cdot 6H_2O$ and H_2BDC] and solvent (DEF or dimethylformamide, DMF) were used, were later developed.   The role of TEA is replaced by diethylamine (DEA) or dimethylamine (DMA) generated from thermal decomposition of solvent:

$$HC(O)NEt_2 + H_2O \rightarrow HCOOH + HNEt_2 \rightleftharpoons HCOO^- + H_2NEt_2^+$$

$$HCOO^- + H_2NEt_2^+ \rightarrow CO_2 + H_2 + HNEt_2$$
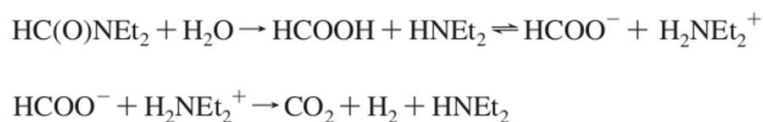
It was found that certain levels of water and proton activity were necessary to obtain MOF-5 rather than other species (also MOFs but derivatives).   Along with the water removing step involved in the decomposition of DMF as illustrated above, the following reactions were also identified to maintain the proton and water at a certain level of reactivity:

acid (formic acid) removing

$$HCOO^- + H_2NEt_2^+ \rightarrow CO_2 + H_2 + HNEt_2$$

water producing

$$HCOOH + HNO_3 \rightarrow CO_2 + HNO_2 + H_2O$$

$$2HCOOH + HNO_3 \rightarrow 2CO_2 + 0.5N_2O + 2H_2O$$
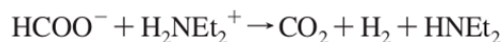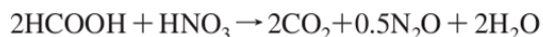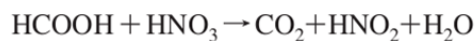
By adjusting the level of proton and water activities through adding water, heating, adding solvent, etc., other Zn-BDC based MOFs can be produced:
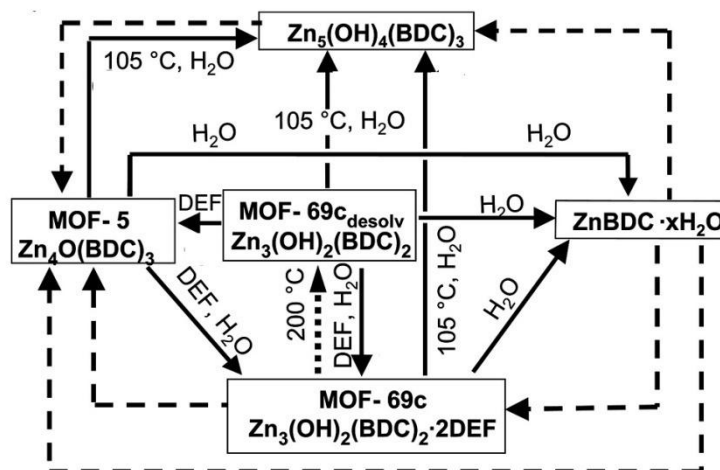
Figure 1.17 Transitions between Zn-BDC based MOFs under solvothermal conditions. The dash lines indicate transitions not available (Hausdorf et al., 2008)

Similar changes in products were also found in the room temperature synthesis with amine. When pH is lowered by changing the ratio of $Zn(NO_3)_2$ and H_2BDC, a change of coordination style from tetragonal to bi-nuclear between zinc ions and BDC groups was also observed. This part will be further illustrated in the chapter of Results and Discussion.

1.6 Objective and outline of this thesis

Here in this thesis work, a method employing the concept of interfacial polymerization in MOF synthesis is introduced. Interfaces, either liquid-liquid or liquid-gas, provide a reactive surface to template in-situ MOF growth. The shape and growth position of MOFs are thus controlled. As a by-product of this proof of concept work, the first free-standing MOF membrane is obtained. We used Zn-BDC based protocols to demonstrate the method. However, the demonstrated concept can find applications far beyond this specific sub-group of MOFs.

In Chapter 1, the background information about MOF membranes is reviewed. This includes already reported methods about MOF membrane fabrication, the principles of interfacial polymerization, and the chemistry of Zn-BDC based MOF formation.

In Chapter 2, the experimental part includes the MOF synthesis in liquid-liquid interface and liquid-gas interface protocol, the fabrication of supported MOF membrane on Anodisc membrane with interfacial coordination and the characterization methods.

In Chapter 3, the results of experiments were presented, analyzed and discussed. Included are the factors that determine the shape of the product in unsupported interfacial synthesis and the morphologies and constitutions of the particles and membranes produced. The gas adsorption test results for the

membranes and particles are also given.

In Chapter 4, the conclusion of this thesis work is made.

In Chapter 5, a personal view on the future of MOFs in general is given.

Chapter 2 Experimental

2.1 Materials

Zinc nitrate hexahydrate [$Zn(NO_3)_2$ $6H_2O$, 99.8%], terephthalic acid (or 1,4-benzene dicarboxylic acid, H_2BDC, 98%), triethylamine (TEA, 98%), dimethylformamide (DMF, 99.8%) and n-hexane (98%) were purchased from Sigma-Aldrich.   Anodisc membranes (0.4 um) were purchased from Walkman.

All chemicals were used as received unless specified in the experimental procedures.

2.2 Experimental procedures

2.2.1 Liquid-liquid interfacial synthesis

In a typical liquid-liquid synthesis protocol, DMF and n-hexane was used as the immiscible solvents.   Zinc nitrate hexahydrate [$Zn(NO_3)_2$ $6H_2O$] and H_2BDC was dissolved in DMF as the precursor solution, denoted as S1.   TEA was dissolved in n-hexane as the deprotonator solution (catalyst solution), denoted as S2.   S2 was added slowly to the top of S1 to allow the reaction to occur at the interface.   The molar ratio of $Zn(NO_3)_2$ $6H_2O$ to H_2BDC was kept constant at 2, which is a typical ratio in Zn-BDC MOF synthesis protocol.   [S1] is denoted as the molar concentration of $Zn(NO_3)_2$ $6H_2O$.   The vial or beaker was sealed to prevent change in TEA concentration resulted from evaporation.

27

The reaction at the interface yielded particles and/or membranes, depending on the precursor and catalyst concentrations, [S1] and [S2].   Membranes were carefully collected by a circle-shaped copper wire as shown in Scheme 2.1.   To avoid unwanted reactions of residual reactants, S2 was carefully taken out from vial in advance with a pipette and the copper wire was raised as fast as possible.   Kim wipe papers were used to absorb the liquid remaining on the membrane.   Then it was put into a vacuum oven to dry at 70 ℃ for 12 hrs.   Since the membrane was further characterized as asymmetric, low temperature, hence a slow drying process was required to avoid the curving of the membrane.

Particles, if produced, were filtered from S1 and washed with DMF 3 times before drying in the vacuum oven for 12 hrs at 70 ℃.   Again, because of the asymmetric structure, this washing process for particles was found not suitable for membranes because it caused curving.
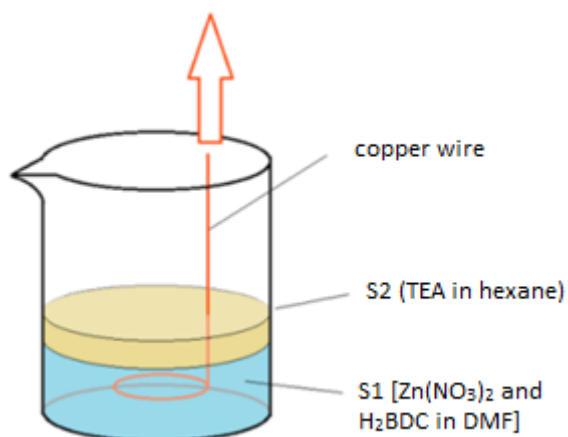
Scheme 2.1 Schematic experiment setup and collection of the membrane samples for liquid-liquid interfacial synthesis

2.2.2 Liquid-gas interfacial synthesis

The procedure of liquid-gas interfacial synthesis was quite similar to that of the liquid-liquid one, except that the catalyst solution was replaced by a saturated TEA vapor. A sealed jar containing liquid TEA was used to create the TEA-saturated atmosphere. A small beaker containing precursor solution (DMF as solvent) having various concentrations was placed in the middle of the jar. The experiment set-up was shown in Scheme 2.2.

Since temperature was kept constant, the vapor pressure of TEA, which is the counterpart of [S2] in the liquid-liquid synthesis protocol, remained unchanged. However, by changing the precursor concentration, i.e. [S1], two different product shapes, membranes and/or particles, could still be produced. The products were collected and processed in the same way as those in the liquid-liquid protocols.
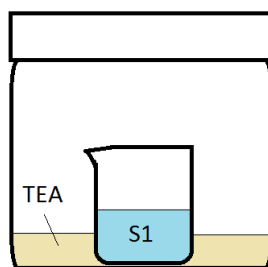
Scheme 2.2 Schematic experiment setup for the liquid-gas interfacial synthesis

2.2.3 Supported MOF membrane synthesis

Both liquid-liquid and liquid-gas approaches were used to grow MOF on Anodisc supporting membranes.   A specially designed glass reactor (shown in Scheme 2.3) was used to carry out the experiments.

In liquid-liquid protocol (Scheme 2.3 a), Anodisc membrane was first mounted between the upper part (catalyst container) and lower part (precursor container) of the reactor.   A sealing washer was used to make sure that the membrane had a tight contact with both sides.   Then the precursor solution was injected from the injection port to the lower part of the reactor until it was in contact with the Anodisc membrane.   In this process, air was expelled out of the pores of Anodisc membrane.   It is important to make sure that the membrane plane is parallel to the solution surface so that the membrane is wetted evenly.   Due to a strong capillary effect, the whole membrane area was wetted very rapidly.   This helped in obtaining an even wetting.   After adding S1, S2 was added slowly along the wall of the upper container to reduce disruption to interface and to expel remaining air at the interface. Then the sealing cap was mounted to avoid evaporation.   After reaction, the membrane was taken out and washed with DMF three times before drying in a vacuum oven for 12 hrs at 70 ℃.

In the liquid gas protocol, adding of S2 in the liquid-liquid protocol was replaced by adding TEA to a small container attached to the upper part of the reactor

(Scheme 2.3 b).   All the other steps were the same.
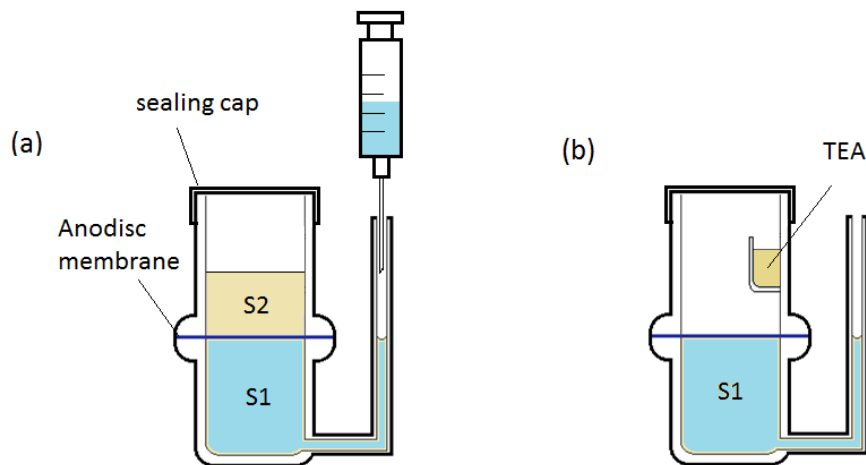
Scheme 2.3 Schematic experiment setup for supported interfacial synthesis. (a): liquid-liquid protocol; (b): liquid-gas protocol

2.3 Characterization

JEOL-7000 Scanning Electronic Microscope was used to study the morphologies of membranes (both supported and unsupported) and particles. A 5 nm platinum coating was introduced to the samples before characterization. Top view, bottom view and cross-section images were obtained for the studied membranes.

The constitutions of non-supported membranes and particles were characterized by X-ray diffraction (XRD) using Bruker D8 Advance Powder Diffractometer. The membranes were scanned from both top view and bottom view for comparative studies.

The gas adsorption properties of both particles and membranes were obtained

by nitrogen adsorption/desorption tests at 77 K using an ASAP 2020 Nitrogen

Adsorption Porosimeter.

Chapter 3 Results and Discussion

3.1 Determination of Product Shapes

In the early experiment, it was found that the product shape varied from membrane to particle with the relative precursor and catalyst concentrations (no catalyst adjustment in liquid-gas protocol). A large number of experiments were conducted to figure out the shape determination windows.

3.1.1 Liquid-liquid Interface Protocol

In the liquid-liquid interface protocol, the precursor solution concentration, [S1] was varied at sixteen levels from 0.025 mol/L to 0.4 mol/L (the concentration of $Zn(NO_3)_2$, while $Zn(NO_3)_2$ to H_2BDC molar ratio remaining constant two) with an increment of 0.025 mol/L, while [S2] was at eight levels ranged from 6.25 to 50 wt% of TEA in hexane with an increment of 6.25 wt%. Three regions were identified where different product shapes were produced. Figure 3.1 shows that the combinations of high [S1] and low [S2] gave membranes while low [S1] and high [S2] yielded particles. Between the membrane and particle regions, there existed a transitional region where both membranes and particles were produced.

Figure 3.2 shows the effect of [S1] variation on the product shape with [S2] fixed to 12.5 wt% TEA. At [S1] $\geq$ 0.25 mol/L, membranes were clearly formed at

the interfaces.   These membranes remained semi-transparent inside the solution.

No visible changes were observed as time proceeded.   At [S1] =0.05, 0.10 and 0.15

mol/L, particles were produced and settled down to the bottom of the vials.   When

S2 was added to the top of S1 at low concentrations, a white/opaque

membrane-shaped interfacial area was formed instantaneously and it was still

observable 10 min later.   As time proceeded, there was white flocculent-like

particulate substance grown from interface into DMF phase, and the DMF phase

became turbid.   It was clear from the vials at t=30 min and 1 hr that higher [S1]

resulted in slower generation of such flocs.   The initially formed membrane-shaped

area was found to separate from the interface at a very slow rate, and finally all the

solid phase was precipitated out and settled to the bottom at t=10 hrs.   At [S1]=0.20

mol/L, no separation of the initially formed area was observed, with particulate and

membrane products coexisting in the final product.   This transitional state was

represented by green triangles in Figure 3.1.   Similar behavior was also observed

with the [S2] variation at a fixed [S1].   Membranes were generated only when [S2]

was lower than some critical value.   Particle precipitation rate increased with

increased [S2].
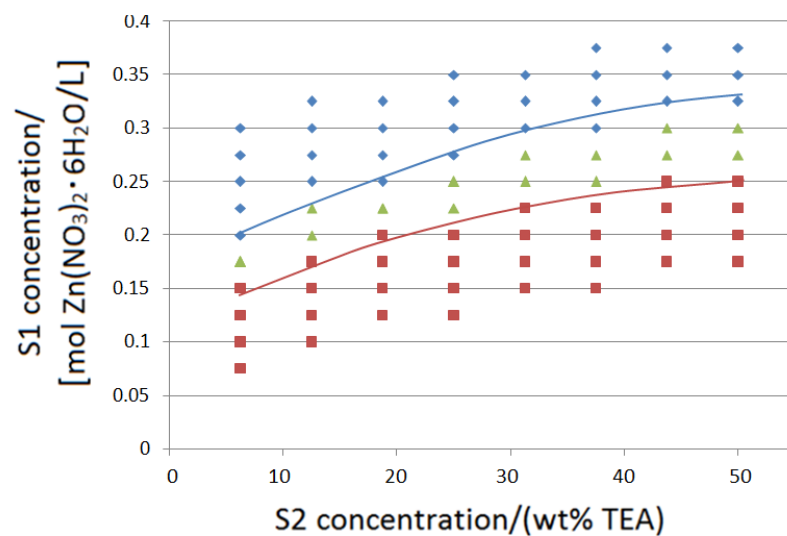
Figure 3.1 Three concentration regions for synthesis of the different product shapes. (◆): only membrane formed, (■): only particles produced and (▲): membrane and particulate products coexisted.
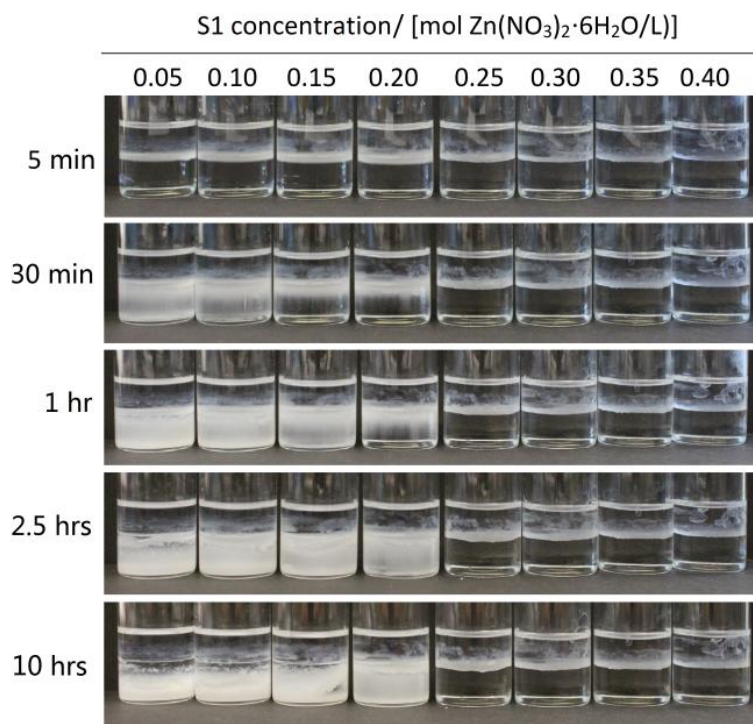
Figure 3.2   The influence of zinc precursor concentration on the product shape. From left to right, [S1] increases from 0.05 to 0.4 mol/L arithmetically with an increment of 0.05 mol/L, while [S2]=12.5 wt% TEA.

The concentration dependence of the product shape can be explained by the different diffusion rates of precursors and TEA and the competition between TEA diffusion and membrane formation process.   Although TEA was miscible with both hexane and DMF, it preferred DMF due to polarity similarity.   Upon addition of S2 to the top of S1, TEA had a strong tendency to penetrate hexane/DMF interface and diffuse into DMF layer.   This diffusion process was enhanced by higher TEA concentration in hexane.   In contrast, there was no such tendency for the precursor species $Zn(NO_3)_2$ and TPA to go into hexane due to their extremely low solubilities. The reaction sites could be either right at the interface or in the DMF phase.   In a typical membrane formation process, two steps were involved, that is, the formation of an initial membrane through networking particles at the interface, followed by the growth of the membrane through growth of the existing particles and nucleation of new particles on the surface of the membrane facing S1.   The first step occurred instantaneously upon the S2 addition.   The initial membrane provided a template for further growth of the membrane.   Also, while the interface was partially sealed by this initial membrane, TEA started to experience diffusion limitations.   The new particles were generated on the surface of membrane rather than inside the DMF phase.

At low [S1] and high [S2] where only particles were produced, the formation of this initial membrane was disturbed.   The reactions between TEA and precursor

species consumed the reactants rapidly at the beginning.   Since TEA was relatively abundant, it outmatched precursor species in diffusion and caused a reaction site moving into the DMF phase.   Therefore, networking of primary particles at the interface would not occur due to their low concentration.   The new particles formed were not concentrated in the interface region.   The observed membrane-shaped areas formed at the beginning were likely to be primary particles or their aggregates held by interfacial tension.   Their white/opaque appearance also revealed that there were cracks and inter-particle spaces larger than visible light wavelengths.   These cracks provided channels for the rapid diffusion of TEA into the DMF phase that generated precipitated particles that settled down to the bottom of the vial.   When large [S1] and small [S2] was used, the precursor consumption was timely compensated at the beginning of the reaction.   The diffusion of TEA was also slowed down because of smaller gradient of concentration.   The initial membrane could thus be formed at the interface and thereafter a membrane product was yielded.

3.1.2 Liquid-gas interface protocol

Since the vapor pressure in the liquid-gas protocol, which is the counterpart of [S2] in the liquid-liquid situation, remained constant under the same room temperature (25 ℃), the only parameter available for adjustment was the precursor concentration [S1].   As shown in Figure 3.3, similar effects of the precursor

concentration on the product shape as those in the liquid-liquid protocol were observed:, that is, low [S1] resulted in particles while high [S1] produced membranes. It is reasonable to assume the same mechanism of diffusion and competition was involved in the MOF formation.   Since the critical S1 concentration of shape transition appeared at 0.2~0.3 mol/L, the reactivity of saturated TEA vapor at the interface matches that of the TEA-hexane solution having a concentration of 25~45 wt% (refer to Figure 3.1).
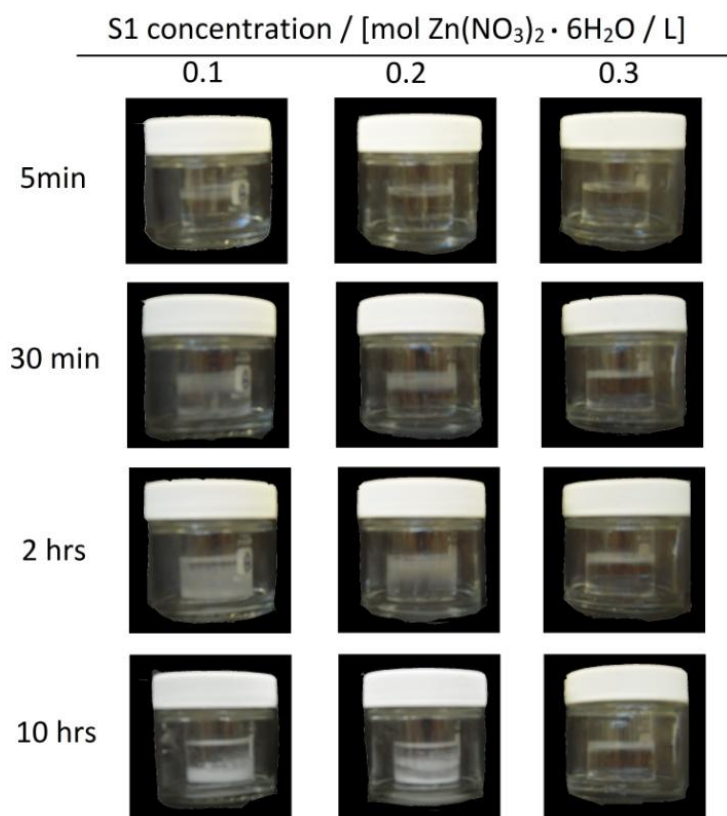
Figure 3.3   The influence of precursor concentration on the product shape. From left to right, [S1] = 0.1, 0.2 and 0.3 mol/L, respectively.

3.2 Morphologies, constitutions and gas adsorption performances

3.2.1 Particles

Figure 3.4 (a) shows a typical example of the morphology of the particles. The sample was taken from the second vial in Figure 3.2 and the reaction time was 90 min.   The size of the particles was around 0.1 um.
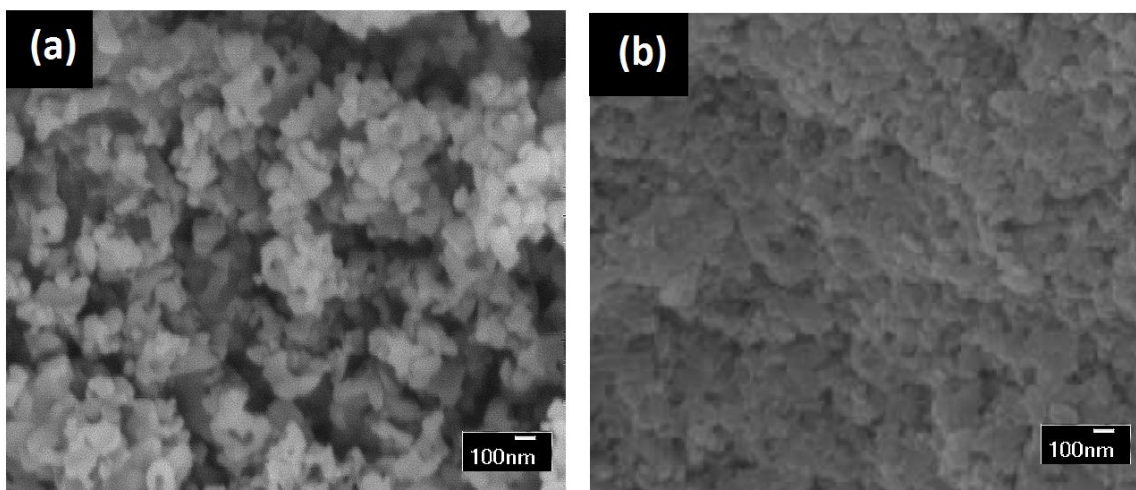
Figure 3.4 SEM images of (a): particles synthesized from interfacial coordination, [S1]=0.1 mol/L, [S2]=12.5 wt% TEA, t=90 min; (b): MOF-5 nano-particles by Huang et al., TEA was added into 0.2 M Zn(NO$_3$) 6H$_2$O-0.1 M H$_2$BDC DMF solution directly with vigorous agitation.

The powder-XRD pattern of the particles shown in Figure 3.5 has peak positions almost identical to the simulated pattern of Zn$_4$O(BDC)$_3$ (known as MOF-5) based on the crystal structure.   The particles were exclusively MOF-5.   The difference in signal intensities was possibly from the size difference -- the particle size obtained in this work was much smaller than those obtained from solvothermal

method (10-500 um).

Nitrogen adsorption/desorption test at 77 K gave the Langmuir surface area of the particles of 2118 ($\pm$29) m^2/g, which is exceptionally high for MOF-5 synthesized under this condition.   The morphology and micro-structure of the particles were compared to those synthesized from the conventional room temperature protocol (Huang et al., 2002), as shown in Figure 3.4 (b) and Table 3.1.   The later was obtained under the same Zn-BDC concentration, but TEA was added in a dropwise manner under vigorous agitation.   The relatively larger particle size explained the smaller external surface area of the particles by the interfacial method than that by the conventional method.   A much larger micropore volume of particles from interfacial method was also observed.   In this method, when the interface was semi-sealed by the newly formed particles, TEA diffusion was reduced and resulted in slower growth of MOF in the interfacial method, where the construction blocks of MOF could be assembled with fewer defects.   This possibly explains the better quality of MOF-5 than those from conventional methods.
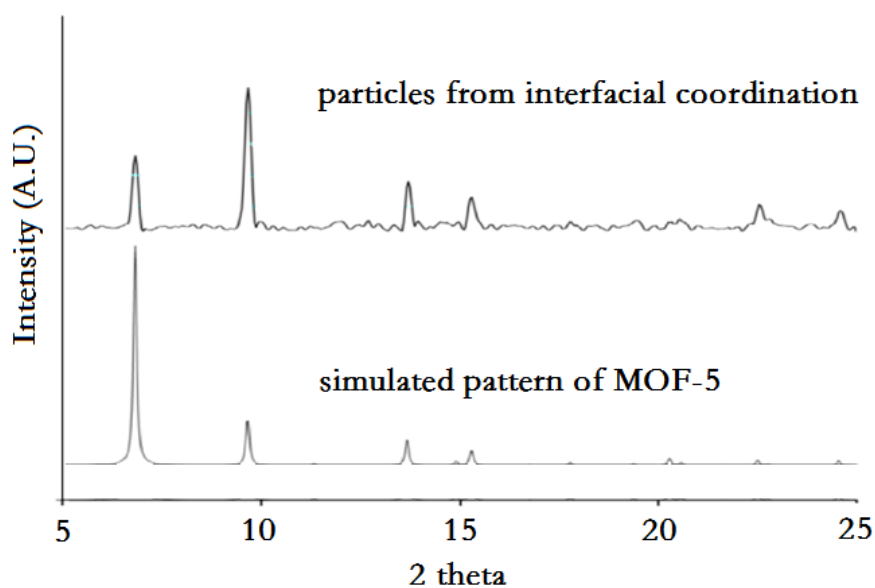
Figure 3.5 PXRD patterns of particles and MOF-5

Table 3.1 Comparison of micro-structures of particles from interfacial coordination and those from adding TEA directly

Method of synthesis	Interfacial coordination	Adding TEA to precursor solutions directly (Huang et al., 2002)
Langmuir surface area (m^2/g)	2118	722
BET surface area (m^2/g)	1919	666
External surface area (m^2/g)	387	535
Micropore Volume (cm^3/g)	0.59	0.21

From the gas-adsorption kinetic curve (Figure 3.6), a sharp increase of nitrogen adsorption at very low nitrogen pressure indicated strong interaction between

41

nitrogen molecules and the MOF material.   After this sharp increase, the adsorption

amount increased very little with the increase of nitrogen pressure up to $P/P_0 > 0.9$.

This suggested that single layer adsorption (Langmuir) was dominating the pressure

range ($P/P_0 < 0.9$) and that the surface was saturated at very low pressure ($P/P_0 < 0.05$).

As low pressure was sufficient to fulfill its adsorption potential, materials with this

kind of absorption kinetic would possess very low gas permeation resistance, which is

ideal for gas separation applications.
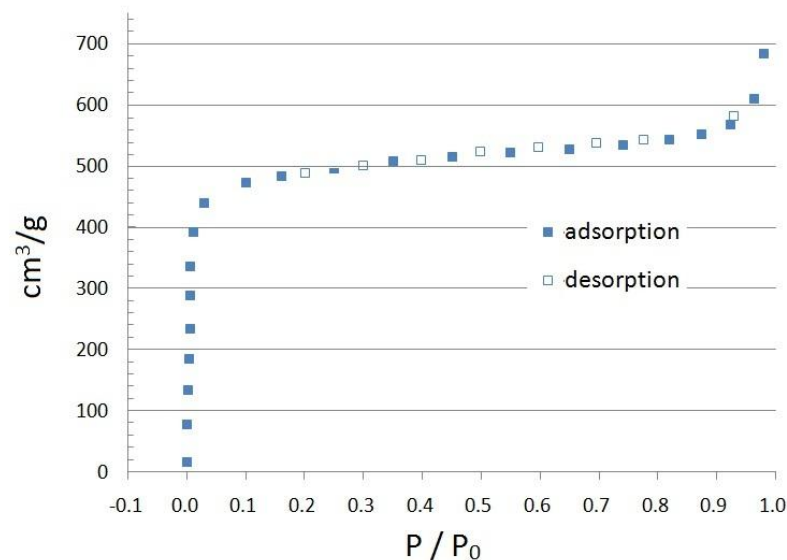
Figure 3.6   Isothermal nitrogen adsorption/desorption curve of the particles, temperature set to 77K.

3.2.2   Free-standing membranes

The combination of high [S1] and low [S2] (or just high [S1] in the liquid-gas

protocol) yielded free-standing MOF membranes (Figure 3.7).   An example of the

membrane morphology was given in Figure 3.8.   The sample was taken from the 8th vial in Figure 3.2 from left to right.   Reaction time was set to 90 min.   Unlike the homogeneous particles, the membranes formed at high [S1] and low [S2] had much more complex morphologies and constitutions.   Figure 3.8 (a) and (c) clearly show different morphologies between top and bottom views of the membrane.   The top layer consisted of particulate structures similar to those particles produced at high [S2] and low [S1] in shape and size.   The bottom layer, however, comprised highly crystallized sheets varying from 5 to 10 um in diameter.   It was found from the cross-section that the major portion of the membrane contained the sheet-like material. The top layer of MOF-5 was very thin and not observable from the cross-section view. There was also a tendency for the sheets to arrange in a perpendicular direction to the membrane plane in the cross-section image.   This suggested a van der Drift growth process for the grains at the bottom of the membrane.

Figure 3.7 Free-standing membrane yielded from high [S2]-low [S1] protocol.
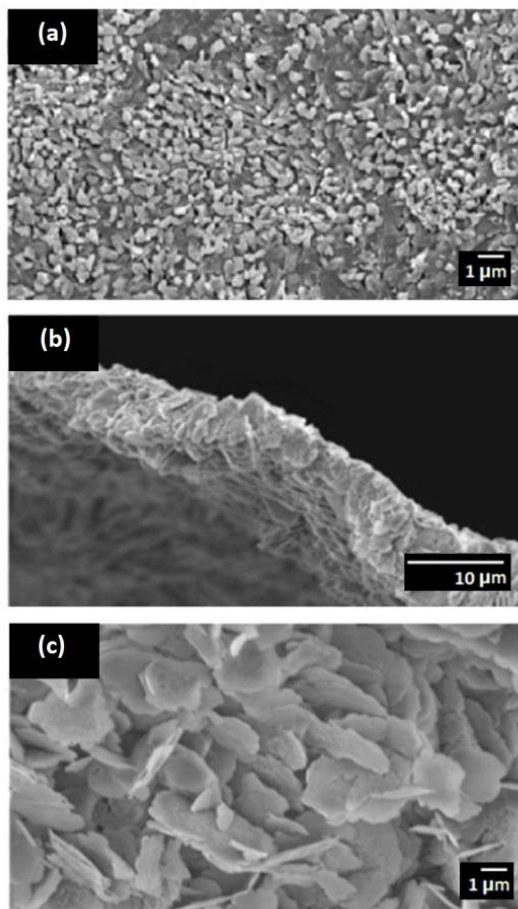
Figure 3.8   SEM images of: (a) top view, (b) cross-section, and (c) bottom view of membrane formed at [S1]=0.4 mol/L, [S2]=12.5 wt% TEA. Reaction time was set to 90 min.

To determine the top and bottom layer compositions, we did XRD characterization from two different directions.   Figure 3.9 (b) and (c) show the results. No scanning tilt was applied because of the small membrane thickness.   From both sides, the signals of the surface layer and middle layer were observed with different signal strength.   By comparison to Figure 3.8 (a), we found that both (b) and (c) contained the typical peaks of ZnBDC·DMF or MOF-2.   This kind of material

consists of square grid 2D layers stacked in an offset manner to accommodate DMF (and/or water) moieties coordinated to zinc ions. (Figure 3.10).   This topology well explained the observed sheet-like shape of bottom material.   The strong intensities of these peaks also agreed with the SEM images that the crystalline sheets were the dominant constitution inside the membrane.   Typical signals of MOF-5 were observed merely on the top scanning of the membrane (Figure 3.9 b, 9.7^0 and 20.3^0); signals of $Zn_3(OH)_2BDC_2$ (also known as MOF-69c) and another MOF, $Zn_5(OH)_4(BDC)_3$ were observed from both top and bottom views (8.4^0, 8.7^0 and 9.2^0) with relatively smaller intensities.   The analysis of these signals was based on comparison to already obtained results in the Zn-BDC MOF system (please see Appendix-XRD for the details).
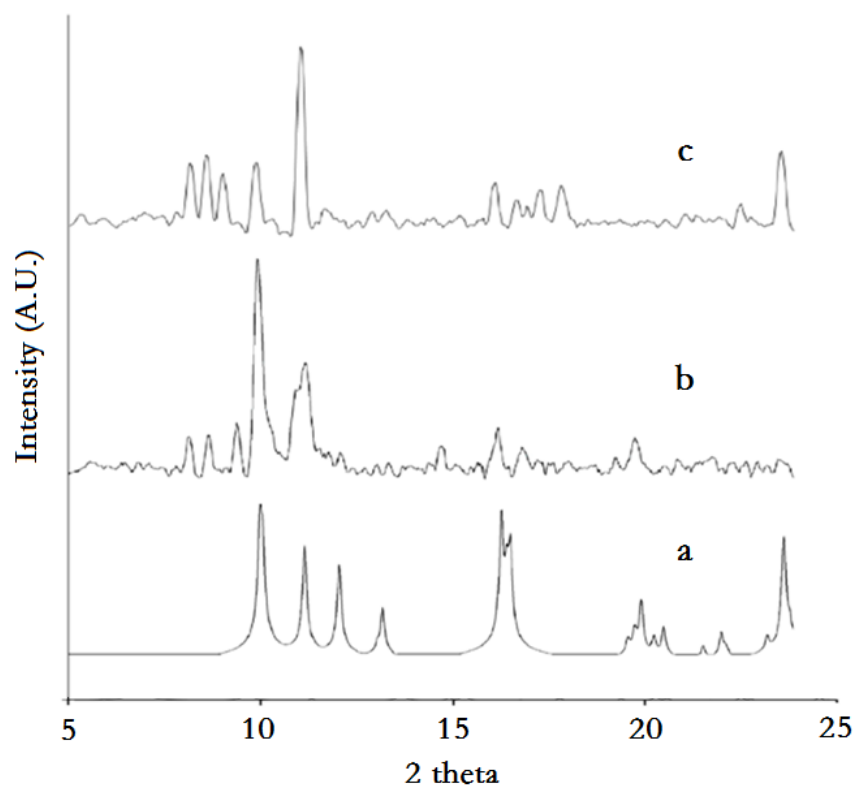
Figure 3.9   XRD patterns: (a) ZnBDC ĐMF (MOF-2) theoretically simulated;[37] (b) from the top of membrane; (c) from the bottom of membrane.
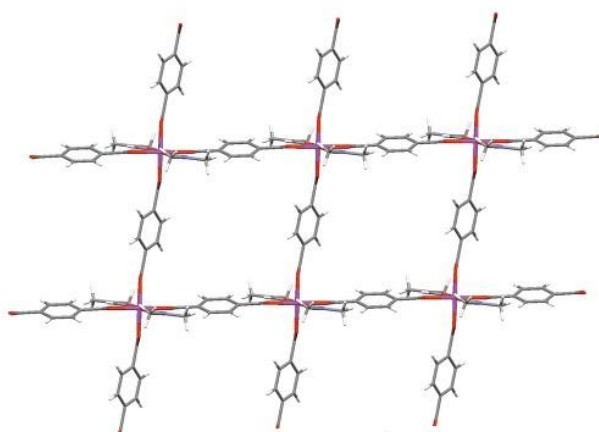
Figure 3.10   Square-grid pattern of MOF-2. Gray: carbon; red: carboxyl group; purple: zinc cluster.

The asymmetrical feature of the membrane in terms of morphology and composition showed a typical effect of pH change in MOF growing condition. When proton activity increased, the coordination between -OH groups and Zn^{2+} to form Zn_4O was no longer feasible because the deprontonation of -OH would not occur at such acidity.   Instead, the coordination between Zn^{2+} and BDC^{2-} groups underwent a transformation from tetrahedron zinc-oxo-BDC to binuclear zinc-BDC-DMF,
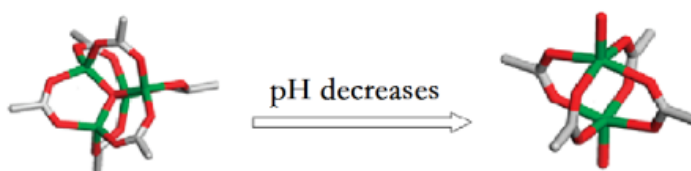
green: zinc, red: oxygen, gray: carbon

Consequently, this transformation resulted in the transition from the cubic-shaped frame to the 2D square-shaped grid in unit cells and thus the transition from 3D MOF-5 to 2D MOF-2 at a macroscopic level.

The direction of membrane growth was the same as that of TEA diffusion, that is, from the interface downward into the DMF phase.   Since TEA is alkaline and TPA is acidic, S1 had a much higher proton activity than S2.   At the initial step of membrane formation, the particles grown in a TEA-rich (or TPA starving) environment had thus the MOF-5 structure because of high pH.   These particles formed the top layer of the membrane.   Upon formation of the initial membrane, TEA experienced diffusion limitations across the membrane.   The reaction site

became TEA-starving (low pH) and MOF-2 was thus formed. This type of MOF material dominated the membrane composition in both cross-section and bottom views of the membrane, as evident in the SEM images. This explanation was also supported by the fact that only MOF-5 was found in the particulate product at the combinations of high [S2] and low [S1], where the MOF material was formed under TEA-rich conditions.

From the isothermal nitrogen adsorption/desorption tests, the average porosities and surface areas of the membrane were measured and summarized in Table 3.2. For comparison, Yaghi has reported a surface area (Langmuir) of about 270 m^2/g and micropore volume of 0.093 cm^3/g for MOF-2. Separating MOF-2 layer from the membrane for an independent surface area test was challenging, if not impossible. However, it is evident that the MOF-2 obtained in this work, which was the primary component of the membrane, was at least comparable to the reported value (note: 709 m^2/g is more than two times of 270 m^2/g).

The gas adsorption kinetic curve of the membrane (Figure 3.11) exhibited a similar pattern as that of the particles, except for less sign of multilayer absorption (BET adsorption). The curve was almost horizontal for $P/P_0 > 0.1$ and remained flat up to P/P_0 ~1. This was possibly because the layer-by-layer stacked pattern of MOF-2 provided little space for multi-layer adsorption.

Table 3.2 Porosities and surface areas of the membrane

Langmuir surface area (m^2/g)	709
BET surface area (m^2/g)	648
External surface area (m^2/g)	57.3
Micropore volume (cm^3/g)	0.23
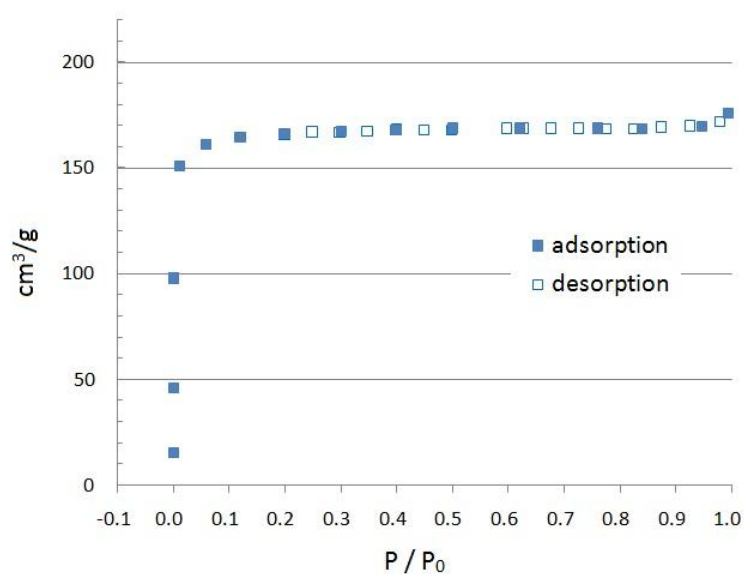
Figure 3.11 Isothermal nitrogen adsorption/desorption curve of the membrane and particles with temperature set to 77K.

3.2.3 MOF membranes on Anodisc substrates

Due to the low thickness (~10 μm) and crystalline composition, it is unlikely that the above unsupported membrane could be directly used for gas separation. However, this technique pointed out a way that the growth position of MOF could be precisely controlled by the interfacial coordination.   As a further demonstration,

supported membranes were synthesized with this interfacial technique.
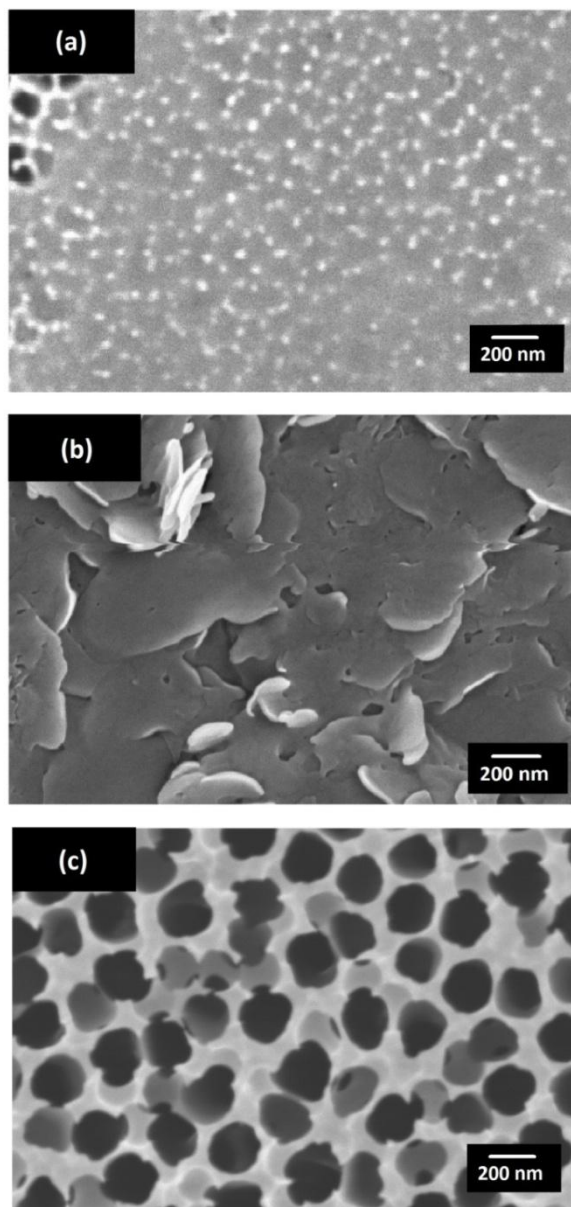
Figure 3.12 Top view of (a): MOF membrane prepared by the liquid-liquid interfacial coordination, (b): MOF membrane by the liquid-gas interfacial coordination and (c): bare surface of Anodisc membrane.

Figure 3.12 gives comparison between the top views of (a) the membrane prepared by the liquid-liquid interfacial coordination on Anodisc, (b) that by the

liquid-gas interfacial coordination on Anodisc, and (c) the bare Anodisc membrane for reference.   In the liquid-liquid protocol (a), the pores were sealed right by the neck of their outlets, while in the liquid-gas protocol (b), a dense and thorough coverage over the substrate membrane was obtained.

From the cross-section SEM, it is found that this MOF layer accounted for a very small thickness and this small layer only appeared on the top of Anodisc. Figure 3.13 shows the cross-section of the liquid-gas protocol sample (corresponding to Figure 3.12 b). Please note: the bottom views of the membranes from both protocols were identical to that of the bare Anodisc membrane and thus are not presented.   Also not shown is the cross-section of the liquid-liquid sample (corresponding to Figure 3.12 a), in which MOF particles inside the top membrane layer were not seen probably because they came off during the sample cutting process.
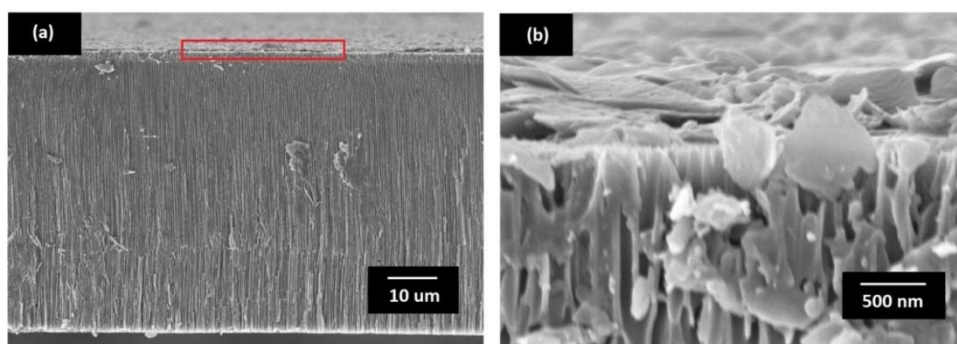
Figure 3.13 (a) MOF layer from the cross-section of Anodisc membrane from the liquid-gas synthesis protocol.   The layer was marked in red; (b) a zoomed-in view of above MOF layer.

The difference between the top morphologies of (a) and (b) in Figure 3.12 and the fact that the MOF layer was only formed on the top of Anodisc could be

explained by the wetting style between the reactant solution and the Anodisc membrane.   The contact angle between DMF and Anodisc alumina was measured to be around 36^0 (Redon et al., 2005), indicating very strong interaction between the precursor solution and the support membrane.   Thus, when the precursor solution was in contact with the pores of the Anodisc membrane, a strong capillary effect was expected.   In the liquid-gas protocol, this capillary effect brought the precursor solution to the top surface of membrane (Figure 3.14 b) and made it as the reaction site upon exposure to the catalyst vapor and, as a result, a thorough MOF coverage of the top of Anodisc membrane was generated (Figure 3.12 b).   On the other hand, the contact angle between hexane and alumina was measured at 62^0, much larger than that between DMF and alumina (therefore a smaller wetting force).   In the liquid-liquid protocol, the interface (i.e., the reaction site) between the precursor and catalyst solutions was located inside the pores (Figure 3.14 a) and thus lead to the MOF formation right at the entrance of Anodisc pores from the top.
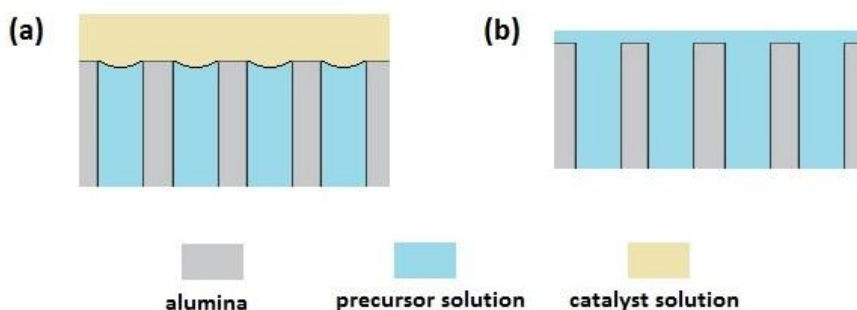
Figure 3.14 Wetting pattern of (a): precursor solution, catalyst solution and Anodisc pores in the liquid-liquid protocol, and (b): precursor solution and Anodisc pores in the liquid-gas protocol

Figure 3.15 shows a larger scale dense and continuous coverage of the MOF layer found on the membrane from the liquid-gas protocol. All Anodisc pores were sealed by this MOF layer adequately. This was also proved by the fact that the precursor solution could not pass through the membrane to the other side, which was tested by simply turning the reactor upside down after the reaction. This kind of morphology is essential for a membrane to function, with no by-pass of gas penetration provided by unsealed pores. However, this thorough sealing was hardly achieved in the liquid-liquid protocol. As shown in Figure 3.12a, open pores existed. This is possibly resulted from small air bubbles formed between two liquid phases when the catalyst solution was added, which hindered the formation of MOF.
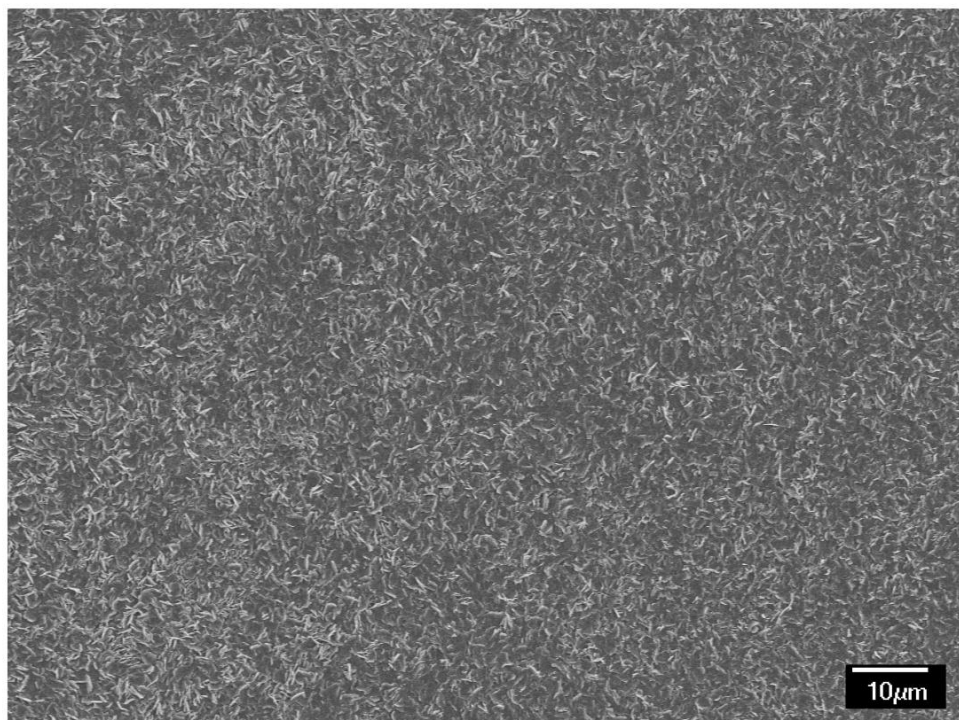
Figure 3.15 Large scale view of the MOF layer from liquid-gas protocol

Chapter 4 Conclusions

This thesis work demonstrated the usefulness of the interfacial coordination method in controlling the growing position and shape of MOFs.   TEA was allowed to react with the precursors of Zn-BDC based MOFs, i.e. zinc nitrate $[Zn(NO_3)_2]$ and terephthalic acid (TPA or H_2BDC) at the liquid-liquid or liquid-gas interface, the formation of the MOF was thereby confined to the precise location of the interface.

In the liquid-liquid interface protocol, there existed three concentration regions.   The combinations of high precursor and low catalyst concentrations yielded membranes, while those of low precursor and high catalyst concentrations produced particles that were precipitated out from the DMF phase.   In between, both membrane and particulate products coexisted.   This was explained by the diffusivity difference between precursor species and TEA across the interface and the competition between MOF formation and TEA diffusion rate.

Similar behavior was found in the liquid-gas protocol -- although TEA vapor pressure remained constant, the change of precursor solution concentration alone resulted in the change of product shapes following the same trends.

The particles formed from both interfaces were identified as exclusively MOF-5.   Much larger internal surface and porosity than those of particles formed in the conventional room temperature method were obtained.   This is possibly because the MOF formed at the interface allowed for a gradual diffusion of TEA into the

precursor solution, hence creating a good MOF growth environment.

The membranes, on the other hand, were found to be asymmetric in both morphology and constitution.   The top layer contained the particulate MOF-5 while the bottom layer and most of cross-section was comprised of disk-like 2D ZnBDC·DMF, i.e. MOF-2.   This was caused by diffusion limitations of TEA crossing the membrane.   The formation of membrane limited the TEA diffusion and the TEA-starving condition on the DMF side changed pH environment for the MOF growth, resulting in the different coordination style between zinc ion and BDC.   The average Langmuir surface area of the membrane was measured to be 709 m^2/g, suggesting pore qualities of the MOF-2 layer at least comparable to those of pure MOF-2.

Both products, the particles and membranes, showed strong interactions with nitrogen molecules at very low pressure, with Langmuir adsorption as the primary gas intake mechanism.

MOF membranes on Anodisc substrates were obtained by applying this interfacial technique to the supported membrane synthesis.   The wetting interactions between substrate material and reactant solutions resulted in thorough coverage of the substrate surface in the liquid-gas protocol and MOF filling into Anodisc pores in the liquid-liquid protocol.   The liquid-gas method gave large scale dense and continuous MOF layers.   Possibly due to the disruption of air bubbles, such continuous MOF layer was rarely observed in the liquid-liquid protocol.

56

Overall, this work showed that the approach of interfacial coordination provided a good control over MOF growing position and shape, which addressed the key engineering issues in the synthesis of MOF based membranes.

Chapter 5   A personal view on the future of MOF

Up to date, there have been plenty of explorations made on MOF applications already, however, I would think that there is still a long way to go to realize the full potentials of these materials.   The most amazing idea that arises from MOF, in my opinion, is that they provide a perfect template to make a functional matrix -- an array of functional areas arranged in a controlled pattern.   The concept is shown in Figure 5.1, where 'A', 'B' and 'C' represent domains with different properties and reactivities. They are introduced to the frameworks of the MOFs by grafting, cage trapping or backbone modification, or by synthesizing a composite crystal containing different types of MOFs.   The size of these domains can range from one unit cell (~10 ångstroms) to micrometer level.   Collectively, they fulfill a certain task in a delicate and well-controlled manner.   This matrix can be fabricated as micro-reactor, molecular sieve, information storage material etc.
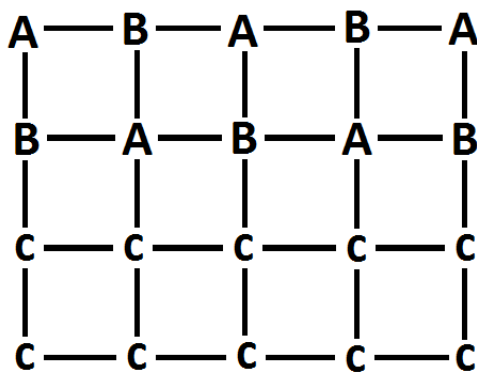
Figure 5.1 The concept of functional matrix. 'A', 'B' and 'C' represent domains with different functionality.

It is said that the development of whole human civilization lies in the reduction of entropy to a lower level, that is, to a more organized pattern of exchanging energy, information and materials.   This process was accompanied by a larger entropy increase beyond our living environment.   Technologically, this means that we can manipulate substance to a smaller and smaller scale and arrange them in the pattern we want, and then build from that base up to whatever level.   Bio-systems are possibly extreme manifestations of such idea, where molecules assemble in such an organized manner, from primary structure (molecules) to secondary structure (3D form of local segments), to tertiary structure (macromolecule folding), all the way up to a life form.   However, engineering of such process is still limited, mostly to introducing functional segments from bio-system to accomplish a certain task.

Engineering of MOFs, is possibly a technology that can reach an organization level closer to that of bio-systems than most of other technologies.   Comparably, we can view the organic bridges (and inorganic ions) as the primary structure of MOF, their assembling into a unit cell as the secondary structure, and the arrangements of different unit cells or cell clusters together at a larger scale as the tertiary structure. The variety of precursors and their assembly styles, and the possibilities in post-synthesis modifications provides unlimited options in function design and processing route design.   Theoretically, the number of domains (functional segments), which can be accommodated into the frameworks, is infinite.   These merits make

MOFs suitable for such matrix development.   In fact, there have already been reports on designing composite MOF materials arranged in multi-layers for gas separation. Despite that this is still at an 'elementary' level compared to the above proposed case, there is hope that the frontier will keep moving forward where the structures can be better manipulated.

References

Adams, R.; Carson, C.; Ward, J.; Tannenbaumb, R.; Koros, W.   Metal organic framework mixed matrix membranes for gas separations, Microporous and Mesoporous Materials 131 (2010) 13–20.

Ameloot, R.; Gobechiya, E.; Uji-i, H.; Martens, J. A.; Hofkens, J.; Alaerts, L.; Sels, B. F.; De Vos, D. E.   Direct Patterning of Oriented Metal–Organic Framework Crystals via Control over Crystallization Kinetics in Clear Precursor Solutions, Adv. Mater. 22 (2010) 2685–2688.

Ameloot, R.; Vermoortele, F.; Vanhove, W.; Roeffaers, M. B. J.; Selsand, B. F.; De Vos, D. E.   Interfacial synthesis of hollow metal–organic framework capsules demonstrating selective permeability, Nature Chemistry 3 (2011) 382-387.

Arnold, M.; Kortunov, P.; Jones, D. J.; Nedellec, Y.; Kärger J.; Caro, J.   Oriented Crystallisation on Supports and Anisotropic Mass Transport of the Metal-Organic Framework Manganese Formate, Eur. J. Inorg. Chem. (2007) 60–64.

Banerjee, M.; Champness, N. R.; Cooper, A. I.; Das, S.; Fischer, R. A.; Jiang, J.; Kim, S.; Kitagawa, S.; Lin, W.; Lin, X.; Ma, L.; Mugnaini, V.; Roques, N.; Schröder, F.; Veciana, J.; Yoon, M.; Uemura, T.; Schröder, M.(Ed) Functional Metal-Organic Frameworks: Gas Storage, Separation and Catalysis, Springer Heidelberg Dordrecht London New York, 2010.

Basu, S.; Cano-Odena, A.; Vankelecom, I. F. J.   Asymmetric Matrimid®/[Cu$_3$(BTC)$_2$] mixed-matrix membranes for gas separations, Journal of Membrane Science 362 (2010) 478–487.

Basu, S.; Cano-Odena, A.; Vankelecom, I. F. J.   MOF-containing mixed-matrix membranes for CO$_2$/CH$_4$ and CO$_2$/N$_2$ binary gas mixture separations, Separation and Purification Technology 81 (2011) 31–40.

Blanita, G.; Lupu, D.; Lazar, M.; Biris, A. R.; Pascalau, V.; Ardelean, I.; Coldea, L.; Misan, I.; Popeneciu, G.; Vlassa, M.   The effect of solution/free volume ratio on the MOF-5 characteristics, Journal of Physics: Conference Series 182 (2009) 012047.

Burrows, A. D.   Mixed-component metal–organic frameworks (MC-MOFs): enhancing functionality through solid solution formation and surface modifications, Cryst. Eng. Comm. 13 (2011) 3623-3642.

Bux, H.; Chmelik, C.; van Baten, J. M.; Krishna, R.; Caro, J.   Novel MOF-Membrane for Molecular Sieving Predicted by IR-Diffusion Studies and Molecular Modeling, Adv. Mater. 22 (2010) 4741–4743.

Bux, H.; Liang, F. Y.; Li, Y. S.; Cravillon, J.; Wiebcke, M.; Caro, J.   Zeolitic Imidazolate Framework Membrane with Molecular Sieving Properties by Microwave-Assisted Solvothermal Synthesis, J. Am. Chem. Soc. 131 (2009) 16000–16001.

Carbonell, C.; Imaz, I.; Maspoch, D.   Single-Crystal Metal -Organic Framework Arrays, J. Am. Chem. Soc. 133 (2011) 2144–2147.

Chae, H. K.; Siberio-Perez, D. K.; Kim, J.; Go, Y. B.; Eddaoudi, M.; Matzger, A. J.; O'Keeffe, M.; Yaghi, O. M.   A route to high surface area, porosity and inclusion of large molecules in crystals, NATURE 427 (2004) 523-527.

Chen, B.; Wang, X. J.; Zhang, Q. F.; Xi, X. Y.; Cai, J. J.; Qi, H.; Shi, S.; Wang, J.; Yuan, D.; Fang, M.   Synthesis and characterization of the interpenetrated MOF-5, 20 (2010) 3758-3767.

Cote, A. P.; Benin, A. I.; Ockwig, N. W.; Keeffe, M. O.; Matzger, A. J.; Yaghi, O. M. Porous, Crystalline, Covalent Organic Frameworks, 310 (2005) 1166-1170.

Dong, A.; Chen, J.; Oh, S. J.; Koh, W. K.; Xiu, F.; Ye, X. C.; Ko, D. K.; Wang, K. L.; Kagan, C. R.; Murray, C. B.   Multiscale Periodic Assembly of Striped Nanocrystal Superlattice Films on a Liquid Surface, Nano Lett. 11 (2011) 841–846.

Dong, A.; Chen, J.; Vora, P. M.; Kikkawa, J. M.; Murray, C. B.   Binary nanocrystal superlattice membranes self-assembled at the liquid – air interface, NATURE 466 (2010) 474-477.

Eddaoudi, M.; Moler, D. B.; Li, H. L.; Chen, B.; Reineke, T. M.; O'Keeffe, M.; Yaghi, O. M.   Modular Chemistry: Secondary Building Units as a Basis for the Design of Highly Porous an Robust Metal -Organic Carboxylate Frameworks, Acc. Chem. Res. 34 (2001) 319-330.

Falcaro, P.; Hill, A. J.; Nairn, K. M.; Jasieniak, J.; Mardel, J. I.; Bastow, T. J.; Mayo, S. C.; Gimona, M.; Gomez, D.; Whitfield, H. J.; Riccò, R.; Patelli, R.; Marmiroli, B.; Amenitsch, H.; Colson, T.; Villanova, L.; Buso, D.   A new method to position and functionalize metal-organic framework crystals, Nature Communications 2 (2011) 1-8.

Gascon, J.; Aguado, S.; Kapteijn, F.   Manufacture of dense coatings of $Cu_3(BTC)_2$ (HKUST-1) on α-alumina, Microporous and Mesoporous Materials 113 (2008) 132–138.

Greathouse, J. A.; Allendorf, M. D.   The Interaction of Water with MOF-5 Simulated by Molecular Dynamics, J. AM. CHEM. SOC. 128 (2006) 10678 -10679.

Guo, H.; Zhu, G.; Hewitt, I. J.; Qiu, S.   "Twin Copper Source" Growth of Metal

-Organic Framework Membrane: $Cu_3(BTC)_2$ with High Permeability and Selectivity for Recycling H_2, J. Am. Chem. Soc. 131 (2009) 1646–1647.

Hafizovic, J.; Bjørgen, M.; Olsbye, U.; Dietzel, P. D. C.; Bordiga, S.; Prestipino, C.; Lamberti, C.; Lillerud, K. P.   The Inconsistency in Adsorption Properties and Powder XRD Data of MOF-5 Is Rationalized by Framework Interpenetration and the Presence of Organic and Inorganic Species in the Nanocavities, J. AM. CHEM. SOC. 129 (2007) 3612 -3620.

Haque, E.; Jeong, J. H.; Jhung, S. H.   Synthesis of isostructural porous metal-benzenedicarboxylates: Effect of metal ions on the kinetics of synthesis, CrystEngComm 12 (2010) 2749–2754.

Hausdorf, S.; Wagler, J.; Mossig, R.; Mertens, F. O. R. L.   Proton and Water Activity-Controlled Structure Formation in Zinc Carboxylate-Based Metal Organic Frameworks, J. Phys. Chem. A, 112 (2008) 7567–7576.

Hawxwell, S. M.; Adams, H.; Brammer, L.   Two-dimensional metal-organic frameworks containing linear dicarboxylates, Acta Cryst. B62 (2006) 808–814, cif file from supporting materials is cited.

Herm, Z. R.; Swisher, J. A.; Smit, B.; Krishnaand R.; Long, J. R.   Metal Organic Frameworks as Adsorbents for Hydrogen Purification and Precombustion Carbon Dioxide Capture, J. Am. Chem. Soc. 133 (2011) 5664–5667.

Hermes, S.; Schröder, F.; Chelmowski, R.; Wöll, C.; Fischer, R. A.   Selective Nucleation and Growth of Metal -Organic Open Framework Thin Films on Patterned $COOH/CF_3$-Terminated Self-Assembled Monolayers on Au(111), J. Am. Chem. Soc. 127 (2005) 13744-13745.

Hermes, S.; Witte, T.; Hikov, T.; Zacher, D.; Bahnmuller, S.; Langstein, G.; Huber, K.; Fischer, R. A.   Trapping Metal-Organic Framework Nanocrystals: An in-Situ Time-Resolved Light Scattering Study on the Crystal Growth of MOF-5 in Solution, J. AM. CHEM. SOC. 129 (2007) 5324 -5325.

Hu, J.; Cai, H.; Ren, H. Q.; Wei, Y. M.; Xu, Z. L.; Liu, H. L.; Hu, Y.   Mixed-Matrix Membrane Hollow Fibers of $Cu_3(BTC)_2$ MOF and Polyimide for Gas Separation and Adsorption, Ind. Eng. Chem. Res. 49 (2010) 12605–12612.

Huang, L.; Wang, H.; Chen, J.; Wang, Z. B.; Sun, J.; Zhao, D. Y.; Yan, Y. S.   Synthesis, morphology control, and properties of porous metal–organic coordination polymers, Microporous and Mesoporous Materials 58 (2003) 105-114.

James, S. L.   Metal-organic frameworks, Chem. Soc. Rev. 32 (2003) 276–288.

Kaye, S. S.; Dailly, A.; Yaghi, O. M.; Long, J. R.   Impact of Preparation and

Handling on the Hydrogen Storage Properties of $Zn_4O(1,4\text{-benzenedicarboxylate})_3$ (MOF-5), J. AM. CHEM. SOC. 129 (2007) 14176 -14177.

Kim, H.; Das, S.; Kim, M. G.; Dybtsev, D. N.; Kim, Y. W.; Kim, K.   Synthesis of Phase-Pure Interpenetrated MOF-5 and Its Gas Sorption Properties, Inorg. Chem. 50 (2011) 3691–3696.

Kim, J.; Chen, B. L.; Reineke, T. M.; Li, H.; Eddaoudi, M.; Moler, D. B.; Keeffe, M.; Yaghi, O. M.   Assembly of Metal-Organic Frameworks from Large Organic and Inorganic Secondary Building Units: New Examples and Simplifying Principles for Complex Structures, J. Am. Chem. Soc. 123 (2001) 8239-8247.

Kim, J.; Chen, B.; Reineke, T. M.; Li, H.; Eddaoudi, M.; Moler, D. B.; O′Keeffe, M.; Yaghi, O. M.   Assembly of Metal -Organic Frameworks from Large Organic and Inorganic Secondary Building Units: New Examples and Simplifying Principles for Complex Structures, J. Am. Chem. Soc. 123 (2001) 8239-8247.

Koh, K. M.; Wong-Foy, A. G.; Matzger, A. J.   A Crystalline Mesoporous Coordination Copolymer with High Microporosity, Angew. Chem. 120 (2008) 689 −692.

Kortunov, P. V.; Heinke, L.; Arnold, M.; Nedellec, Y.; Jones, D. J.; Caroand, J.; Kärger, J.   Intracrystalline Diffusivities and Surface Permeabilities Deduced from Transient Concentration Profiles: Methanol in MOF Manganese Formate, J. Am. Chem. Soc. 129 (2007) 8041-8047.

Li, H. L.; Davis, C. E.; Groy, T. L.; Kelley, D. G.; Yaghi, O. M.   Coordinatively Unsaturated Metal Centers in the Extended Porous Framework of $Zn_3(BDC)_3$ $6CH_3OH$, J. Am. Chem. Soc. 120 (1998) 2186-2187.

Li, H. L.; Eddaoudi, M.; Keeffe, M.; Yaghi, O. M.   Design and synthesis of an exceptionally stable and highly porous metal-organic framework, Nature, 402 (1999), 18-19, crystallography data from supporting files is cited.

Li, H.; Davis, C. E.; Groy, T. L.; Kelley, D. G.; Yaghi, O. M.   Design and synthesis of an exceptionally stable and highly porous metal-organic framework, J. Am. Chem. Soc. 120 (1998) 2186–2187.

Li, J. P.; Cheng, S. J.; Zhao, Q.; Long, P. P.; Dong, J. X.   Synthesis and hydrogen-storage behavior of metal–organic framework MOF-5, International journal of hydrogen energy 34 (2009) 1377–1382.

Li, J. R.; Kuppler, R. J.; Zhou, H. C.   Selective gas adsorption and separation in metal–organic frameworks, Chem.Soc.Rev. 38 (2009) 1477–1504.

Li, Y. S.; Bux, H.; Feldhoff, A.; Li, G. L.; Yang, W. S.; Caro, J.   Controllable Synthesis of Metal-Organic Frameworks: from MOF nanorods to oriented MOF

membranes, Adv. Mater. 22 (2010) 3322-3326.

Li, Y. S.; Liang, F. Y.; Bux, H.; Feldhoff, A.; Yang, W. S.; Caro, J.   Molecular Sieve Membrane: Supported Metal–Organic Framework with High Hydrogen Selectivity, Angew. Chem. Int. Ed. 49 (2010) 548 –551.

Li, Y. S.; Liang, F. Y.; Bux, H.; Yang, W. S.; Caro, J.   Zeolitic imidazolate framework ZIF-7 based molecular sieve membrane for hydrogen separation, Journal of Membrane Science 384 (2010) 48-54.

Liao, J. H.; Lee, T.; Su, C. T.   Synthesis and characterization of a porous coordination polymer, $Zn_5(OH)_4(BDC)_3$ 2DMF (DMF=N,N-dimethylformamide), Inorganic Chemistry Communications 9 (2006) 201–204.

Liao, J.; Zhou, Y.; Huang, C. L.; Wang, Y.; Peng, L. M.   Fabrication, Transfer, and Transport Properties of Monolayered Freestanding Nanoparticle Sheets, Small 7 (2011), 583–587.

Liu, X. L.; Li, Y. S.; Zhu, G. Q.; Ban, Y.; Xu, L.; Yang, W.   An Organophilic Pervaporation Membrane Derived from Metal–Organic Framework Nanoparticles for Efficient Recovery of Bio-Alcohols, Angw. Chem. Int. Ed. 50 (2010) 10636-10639.

Liu, Y.; Ng, Z.; Khan, E. A.; Jeong, H. K.; Ching, C. B.; Lai, Z. P.   Synthesis of continuous MOF-5 membranes on porous α-alumina substrates, Microporous and Mesoporous Materials 118 (2009) 296–301.

Makiura, R.; Kitagawa, H.   Porous Porphyrin Nanoarchitectures on Surfaces, Eur. J. Inorg. Chem. 3 (2010) 3715–3724.

Makiura, R.; Motoyama, S.; Umemura, Y.; Yamanaka, H.; Sakata, O.; Kitagawa, H.   Surface nano-architecture of a metal–organic framework, Nature Materials 9 (2010) 565-571.

Makiura, R.; Tsuchiyama, K.; Sakata, O.   Self-assembly of highly crystalline two-dimensional MOF sheets on liquid surfaces, CrystEngComm 13 (2011) 5538-5541.

Meek, S. T.; Greathouse, J. A.; Allendorf, M. D.   Metal-Organic Frameworks: A Rapidly Growing Class of Versatile Nanoporous Materials, Adv. Mater. 23 (2011) 249–267.

Morris, R. E.   Metal-organic frameworks: grown into shape, Nature Chemistry 3 (2011) 347-348.

Motoyama, S.; Makiura, R.; Sakata, O.; Kitagawa, H.   Highly Crystalline Nanofilm by Layering of Porphyrin Metal-Organic Framework Sheets, J. Am. Chem. Soc.

133 (2011) 5640 –5643.

Mueller, U.; Schubert, M.; Teich, F.; Puetter, H.; Schierle-Arndt, K.; Pastre, J. Metal–organic frameworks — prospective industrial applications, J. Mater. Chem. 16 (2006) 626–636.

Nan, J. P.; Dong, X. L.; Wang, W. J.; Jin, W. Q.; Xu, N. P. Step-by-Step Seeding Procedure for Preparing HKUST-1 Membrane on Porous α-Alumina Support, Langmuir 27 (2011) 4309–4312.

O'Brien, M. G.; Sanchez-Sanchez, M.; Beale, A. M.; Lewis, D. W.; Sankar, G.; Richard, C.; Catlow, A. Effect of Organic Templates on the Kinetics and Crystallization of Microporous Metal-Substituted Aluminophosphates, J. Phys. Chem. C 111 (2007) 16951-16961.

Perez, E. V.; Balkus, K. J.; Jr., Ferraris, J. P.; Musselman, I. H. Mixed-matrix membranes containing MOF-5 for gas separations, Journal of Membrane Science 328 (2009) 165–173.

Purewal, J. J.; Liu, D.; Yang, J.; Sudik, A.; Siegel, D. J.; Maurer, S.; Muller, U. Increased volumetric hydrogen uptake of MOF-5 by powder densification, International journal of hydrogen energy xxx (2011) 1-5.

Ravon, U.; Savonnet, M.; Aguado, S.; Domine, M. E.; Janneau, E.; Farrusseng, D. Engineering of coordination polymers for shape selective alkylation of large aromatics and the role of defects, Microporous and Mesoporous Materials 129 (2010) 319–329.

Shekhah, O.; Liu, J.; Fischer, R. A.; Woll, C. MOF thin films: existing and future applications, Chem. Soc. Rev. 40 (2011) 1081–1106.

Shekhah, O.; Wang, H.; Kowarik, S.; Schreiber, F.; Paulus, M.; Tolan, M.; Sternemann, C.; Evers, F.; Zacher, D.; Fischer, R. A.; Wöll, C. Step-by-Step Route for the Synthesis of Metal-Organic Framework, J. AM. CHEM. SOC. 129 (2007) 15118 -15119.

Surble, S.; Millange, F.; Serre, C.; Ferey, G.; Walton, R. I. An EXAFS study of the f ormation of a nanoporous metal–organic framework: evidence f or the retention of secondary building units during synthesis, Chem. Commun. (2006) 1518–1520.

Tachikawa, T.; Choi, J. R.; Fujitsuka, M.; Majima, T. Photoinduced Charge-Transfer Processes on MOF-5 Nanoparticles: Elucidating Differences between Metal-Organic Frameworks and Semiconductor Metal Oxides, J. Phys. Chem. C 112 (2008) 14090–14101.

Tanabe, K. K.; Cohen, S. M. Postsynthetic modification of metal–organic frameworks—a progress report, Chem. Soc. Rev. 40 (2011) 498–519.

Vairaprakash, P.; Ueki, H.; Tashiro, K.; Yaghi, O. M.   Synthesis of Metal-Organic Complex Arrays, J.A.C.S., (2010).

Xin, Z. F.; Bai, J. F.; Pan, Y.; Zaworotko, M. J.   Synthesis and Enhanced H_2 Adsorption Properties of a Mesoporous Nanocrystal of MOF-5: Controlling Nano-/Mesostructures of MOFs To Improve Their H_2 Heat of Adsorption, Chem. Eur. J. 16 (2010) 13049 – 13052.

Yaghi, O. M.; O'Keeffe, M.; Ockwig, N. W.; Chae, H. K.; Eddaoudi, M.; Kim, J.   Reticular synthesis and the design of new materials, NATURE 423 (2003) 705-714.

Yoo, Y.; Jeong, H. K.   Rapid fabrication of metal organic framework thin films using microwave-induced thermal deposition, Chem. Commun. (2008) 2441–2443.

Yoo, Y.; Lai, Z.; Jeong, H. K.   Fabrication of MOF-5 membranes using microwave-induced rapid seeding and solvothermal secondary growth, Microporous and Mesoporous Materials 123 (2009) 100–106.

Zacher, D.; Baunemann, A.; Hermes, S.; Fischer, R. A.   Deposition of microcrystalline [$Cu_3(btc)_2$] and [$Zn_2(bdc)_2(dabco)$] at alumina and silica surfaces modified with patterned self assembled organic monolayers: evidence of surface selective and oriented growth, J. Mater. Chem. 17 (2007) 2785–2792.

Zhang, L.; Hu, Y.   Structure distortion of $Zn_4O_{13}C_2H_{12}$ framework (MOF-5), Materials Science and Engineering B176 (2011) 573–578.

Zhang, L.; Hu, Y. H.   A Systematic Investigation of Decomposition of Nano $Zn_4O(C_8H_4O_4)_3$ Metal-Organic Framework, J. Phys. Chem. C 114 (2010) 2566–2572.

Zhao, D.; Timmons, D. J.; Yuan D. Q.; Zhou, H. C.   Tuning the Topology and Functionality of Metal-Organic Frameworks by Ligand Design, Accounts of Chemical Research 44 (2011) 123–133.

Zhou, Y. X.; Shen, X. Q.; Du, C. X.; Wu, B. L.; Zhang, H. Y.   1D, 2D and 3D Coordination Polymers of Aromatic Carboxylate Tb (III): Structure, Thermolysis Kinetics and Fluorescence, Eur. J. Inorg. Chem. (2008) 4280–4289.

Appendix - Referential XRD Patterns on MOF Types

1. Ravon, U.; Savonnet, M.; Aguado, S.; Domine,   M. E.; Janneau, E.; Farrusseng, D. Engineering of coordination polymers for shape selective alkylation of large aromatics and the role of defects, Microporous and Mesoporous Materials 129 (2010) 319–329.
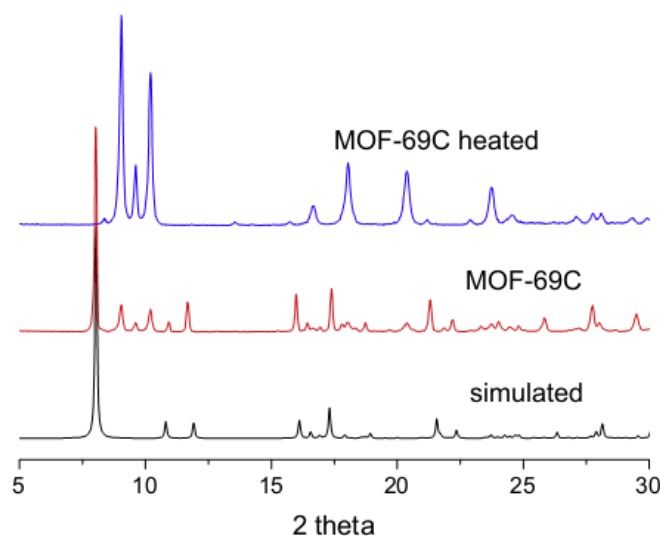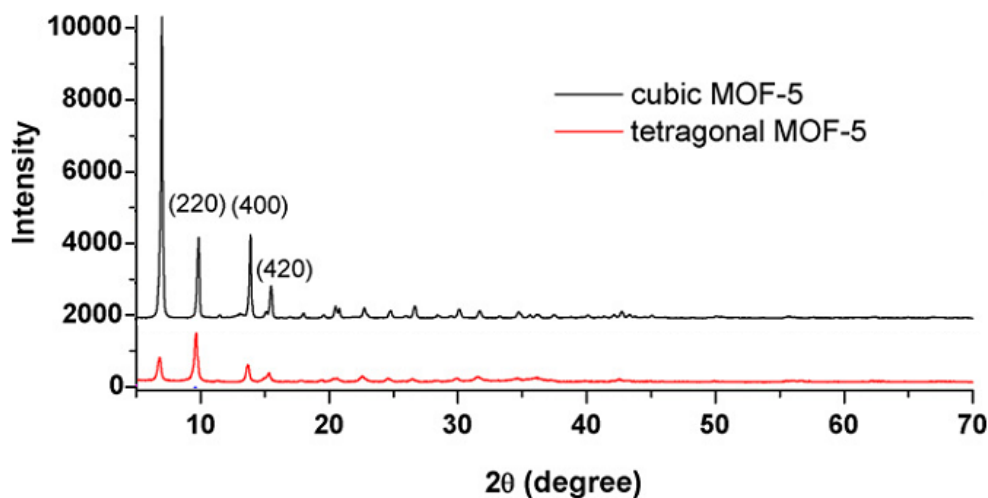

Fig. 5   Powder X-ray diffraction patterns of simulated MOF-69C (bottom), $Zn_3(OH)_2(bdc)_2 \cdot 2DEF$ (MOF-69C) (center), and of $Zn_3(OH)_2(bdc)_2 \cdot DEF$ (top).

2.   Zhang, L.; Hu, Y.   Structure distortion of $Zn_4O_{13}C_{24}H_{12}$ framework (MOF-5), Materials Science and Engineering B176 (2011) 573–578.

Fig. 2. (b) XRD patterns of cubic and tetragonal MOF-5s

3. Liao, J. H.; Lee, T. J.; Su, C. T. Synthesis and characterization of a porous coordination polymer, $Zn_5(OH)_4(BDC)_3 \cdot 2DMF$ (DMF = N,N -dimethylformamide)
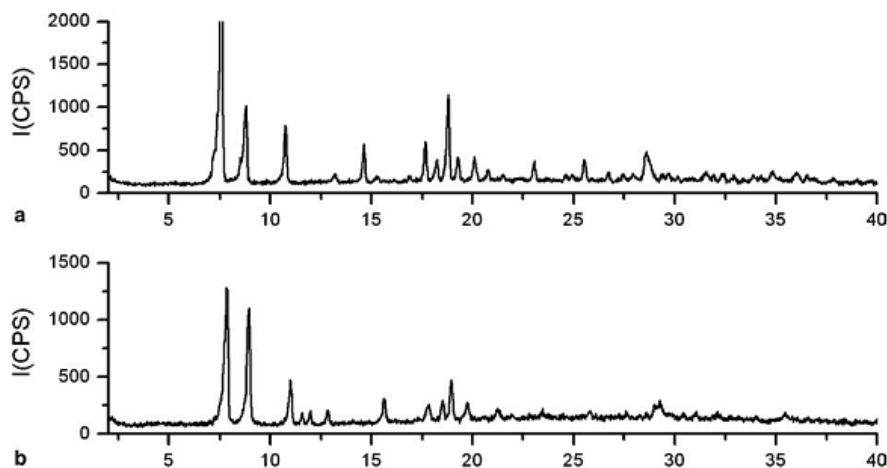

Fig. 5. (a) X-ray powder diffraction pattern of 1 as-synthesized. (b) XRPD of 1 heated to 180 ^{0}C.

4. Hawxwell, S. M.; Adams, H.; Brammer, L. Two-dimensional metal-organic frameworks containing linear dicarboxylates, Acta Cryst. B62 (2006) 808–814. Based on the cif file provided, XRD of 2D MOFs were calculated as:
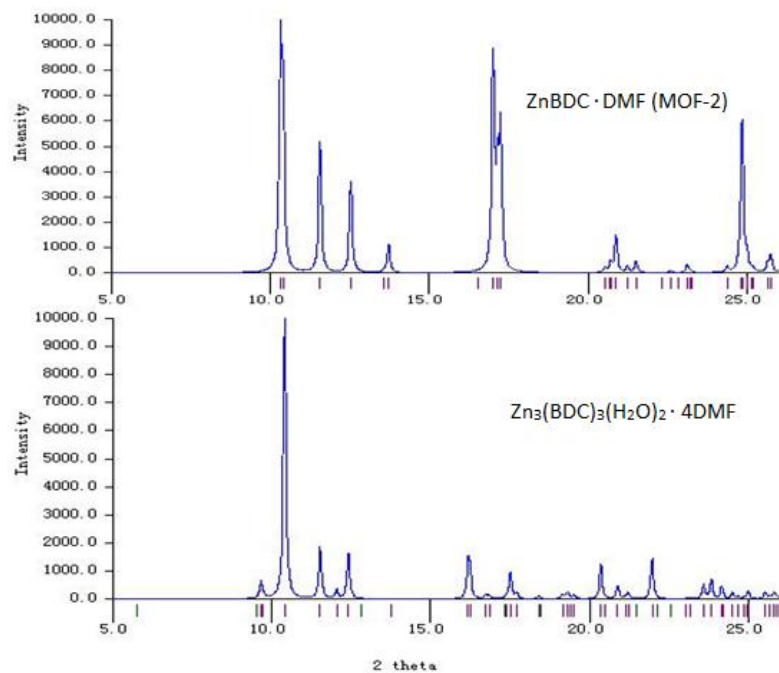

Figure Simulated pattern of MOF-2 and $Zn_3(BDC)_3(H_2O)_2 \cdot 4DMF$ (Variant of MOF-2 with different coordinates)

68

5. Li, J.; Cheng, S.; Zhao, Q.; Long, P.; Dong, J.   Synthesis and hydrogen-storage behavior of metal–organic framework MOF-5, international journal of hy drogen energy 34 (2009) 1377–1382.
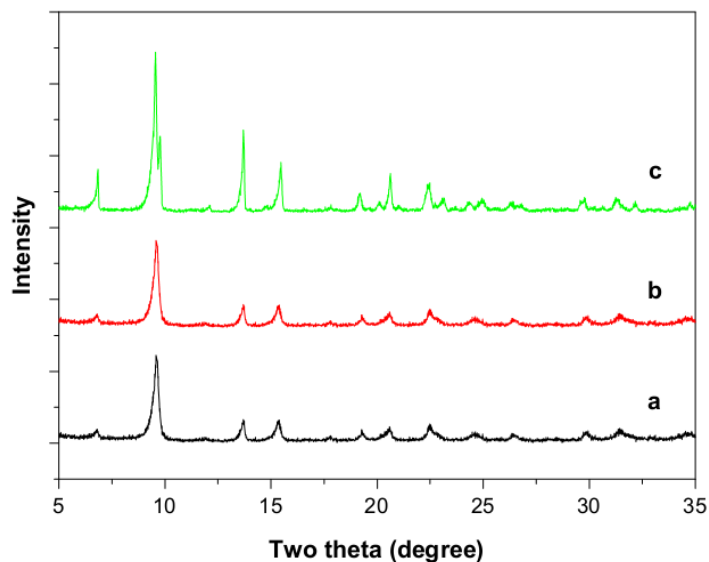

Fig. 1 – XRD patterns of MOF-5 samples produced by: (a) direct mixing of TEA; (b) slow diffusion of TEA; (c) solvothermal synthesis.

6.   Kim, H.; Das, S.; Kim, M. G.; Dybtsev, D. N.; Kim, Y.; Kim, K.   Synthesis of Phase-pure Interpenetrated MOF-5s and Their Gas Adsorption Properties, Inorg. Chem. 50 (2011) 3691–3696.
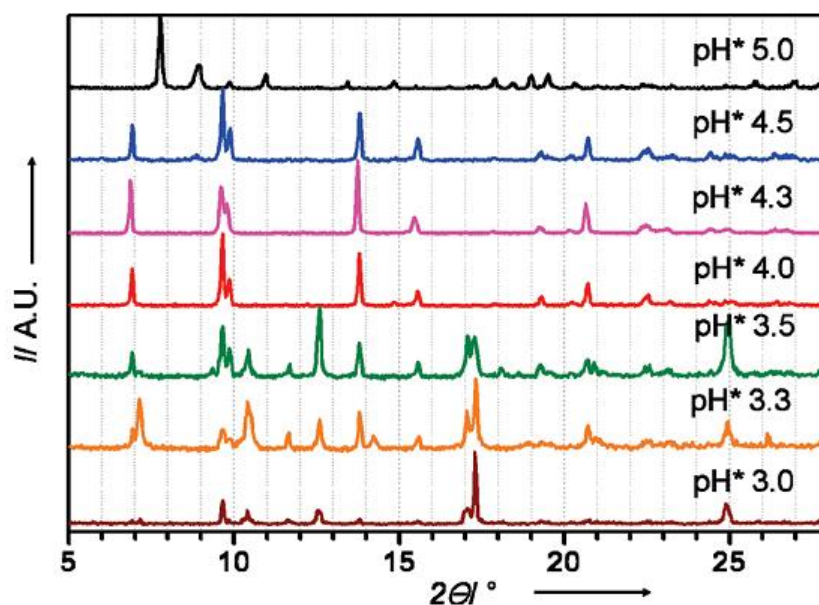

Figure 4. Powder X-ray di ffraction (PXRD) spectra of crystalline materials obtained at di fferent pH values

7.   Huang, L. M.; Wang, H. T.; Chen, J. X.; Wang, Z. B.; Sun, J. Y.; Zhao, D. Y.; Yan, Y.-S.   Synthesis, morphology control, and properties of porous metal–organic coordination polymers, Microporous and Mesoporous Materials 58 (2003) 105–114.
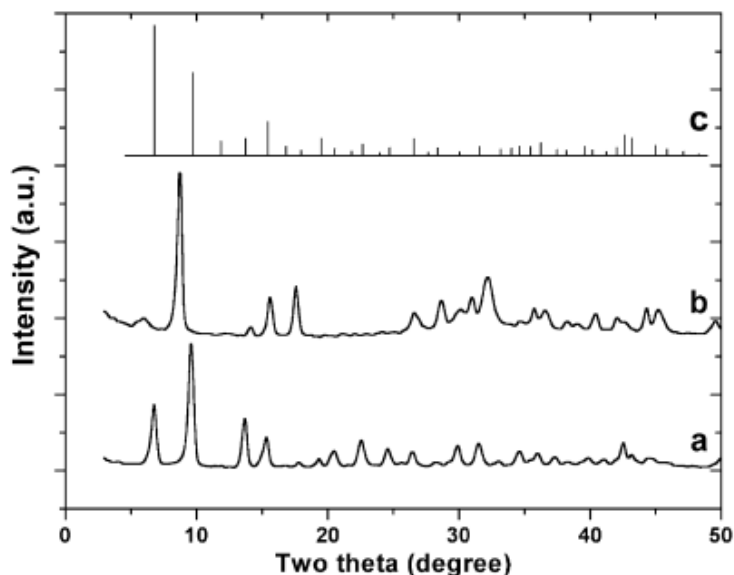

Fig. 2. XRD patterns of: (a) MOCP-L nanocrystals; (b) MOCP-H nanocrystals and (c) simulated XRD pattern for MOF-5 crystal.

8.   Blanita, G.; Lupu, D.; Lazar, M.; Biris, A. R.; Pascalau, V.; Ardelean, O.; Coldea, I.; Misan, I.; Popeneciu, G.; Vlassa, M.   The effect of solution/free volume ratio on the MOF-5 characteristics, Journal of Physics: Conference Series 182 (2009) 012047.
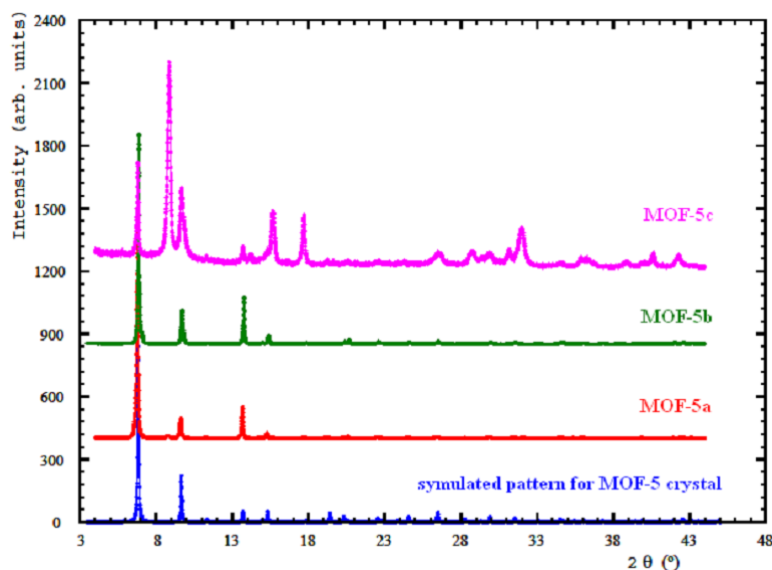

Figure 1. XRD patterns of MOF-5a, MOF-5b, MOF-5c and simulated XRD pattern for MOF-5 crystal.